A Practical Guide to Surface Kinetic Monte Carlo Simulations

Mie Andersen[1*], Chiara Panosetti[1], Karsten Reuter[1]

[1]Technische Universität München, Germany

A Practical Guide to Surface Kinetic Monte Carlo Simulations

Mie Andersen [1,*]**, Chiara Panosetti** [1] **and Karsten Reuter** [1]

[1]*Chair for Theoretical Chemistry and Catalysis Research Center, Technische Universität München, Garching, Germany.*

Correspondence*:
Lichtenbergstr. 4, D-85747 Garching, Germany.
mie.andersen@ch.tum.de

2 ABSTRACT

3 This review article is intended as a practical guide for newcomers to the field of kinetic Monte Carlo
4 (KMC) simulations, and specifically to lattice KMC simulations as prevalently used for surface
5 and interface applications. We will provide worked out examples using the `kmos` code, where
6 we highlight the central approximations made in implementing a KMC model as well as possible
7 pitfalls. This includes the mapping of the problem onto a lattice and the derivation of rate constant
8 expressions for various elementary processes. Example KMC models will be presented within the
9 application areas surface diffusion, crystal growth and heterogeneous catalysis, covering both
10 transient and steady-state kinetics as well as the preparation of various initial states of the system.
11 We highlight the sensitivity of KMC models to the elementary processes included, as well as to
12 possible errors in the rate constants. For catalysis models in particular, a recurrent challenge is
13 the occurrence of processes at very different timescales, *e.g.* fast diffusion processes and slow
14 chemical reactions. We demonstrate how to overcome this timescale disparity problem using
15 recently developed acceleration algorithms. Finally, we will discuss how to account for lateral
16 interactions between the species adsorbed to the lattice, which can play an important role in all
17 application areas covered here.

18 **Keywords: kinetic Monte Carlo, lattice gas model, surface diffusion, heterogeneous catalysis, crystal growth, sensitivity analysis,**
19 **lateral interactions**

1 INTRODUCTION

20 As the witty name suggests, Monte Carlo is a wide umbrella term that covers a numerous family of
21 approaches with one simple central idea in common: the resolution of complex problems using random
22 numbers. Given the versatility of the concept, it is no surprise that Monte Carlo based approaches have
23 gained popularity in computational chemistry and materials science (*cf. e.g.* Frenkel and Smit (2001)),
24 most prominently for the simulation of ensemble properties using Metropolis Monte Carlo, or methods
25 derived from the latter such as Basin Hopping for global geometry optimization. In addition to *equilibrium*
26 properties, the Monte Carlo idea can also be exploited to tackle *dynamical* properties. In this sense, a
27 number of approaches emerged over the decades under different names, until the term kinetic Monte Carlo
28 (KMC) became universally used in this context.

29 Nowadays KMC is a popular tool to describe a variety of phenomena related to *e.g.* transport (diffusion),
30 structures and properties of materials (*e.g.* crystal growth) or equilibrium and non-equilibrium chemistry

31 (catalysis). As will become apparent throughout the text, in the context of atomistic simulations KMC
32 can be considered as a form of coarse graining. This renders it particularly suitable to find its place in
33 hierarchical multiscale modeling approches, where information at different levels of accuracy or detail is
34 integrated to provide a more comprehensive description. In this context, KMC is an essential method to
35 bridge the gap between the microscopic world (elementary processes such as atomistic diffusion jumps or
36 the making and breaking of chemical bonds) and the meso- to macroscopic world (*e.g.* a diffusion constant
37 or a reaction rate).

38 Let us illustrate this concept by considering for example heterogeneous catalysis, which is one of the
39 fields where KMC, as well as hierarchical approaches in general, have made considerable impact Sabbe
40 et al. (2012); Reuter (2016). The design of a catalytic process requires a deep understanding of phenomena
41 ranging from the reactive chemistry to the optimization of heat and mass transport within the reactor.
42 Numerical simulations have become an integral part in this design process, which requires appropriate
43 models at multiple time and length scales, and perhaps most importantly, concepts on how these models
44 should be connected. One can imagine "zooming in" from the macroscopic world where we live and an
45 industrial reactor operates, all the way down to the microscopic scale where the events are ultimately
46 governed by electronic structure: adsorption and desorption of atoms and molecules at surfaces, diffusion,
47 bond breaking and bond forming (see Fig. 1). All of the latter constitute elementary processes that can occur
48 at the interface between the catalyst and the reaction fluid, and can nowadays be described individually to a
49 great level of detail by first-principles electronic structure calculations. At this scale, what one essentially
50 needs is a mechanistic description in terms of the Potential Energy Surface (PES) of the system (*vide
51 infra*). Hereby, an appropriate quantum mechanical approach is required to capture chemical subtleties in a
52 predictive manner. The workhorse for this remains to this day largely Density-Functional Theory (DFT)
53 Hohenberg and Kohn (1964); Kohn and Sham (1965), thanks to its unique compromise between accuracy
54 and efficiency that allows to access system sizes as relevant for heterogeneous catalysis.

55 If one now "zooms out" a little and into the mesoscopic scale, one can see how what globally happens is
56 the result of an intricate interplay of the above elementary processes as well as the interaction with the
57 surrounding environment. Here, the spatiotemporal evolution at the interface is dominated by collective
58 behavior; dynamics and thermodynamics come into play. At this stage, one may employ the microscopic
59 information (*e.g.* reaction barriers, adsorption energies etc. of the elementary processes) and embed it into
60 microkinetic models as a form of coarse-graining. A plethora of approaches of different complexity are
61 available, from Sabatier analysis to mean-field models and kinetic Monte Carlo. Finally, at the macroscale,
62 one needs to take into account transport phenomena and gradients of mass and temperature in the reactor
63 geometry. This is a realm that is presently largely covered by continuum-type fluid dynamical models
64 Janardhanan and Deutschmann (2011). At this stage, again the information from the lower scales can be
65 embedded, *i.e.* here the outcome of the microkinetic models is integrated as an input, for instance in form
66 of a boundary condition to the differential equations describing the flow phenomena Matera and Reuter
67 (2010); Matera et al. (2014). The development of appropriate hierarchical models to effectively describe
68 events at such different scales, and more so of "bridges" to transfer information between them, constitutes
69 the core of modern multiscale modeling approaches (*cf.* Ref. Raimondeau and Vlachos (2002); Reuter et al.
70 (2005); Vlachos (2012)).

71 Similar kind of multiscale approaches have been or are being developed in many other areas of chemistry
72 and materials sciences. Microkinetic models, and there prominently KMC simulations, are generally the
73 approach used to capture the statistical interplay between elementary processes whenever the mesoscopic
74 property or functionality to be described is outside of thermodynamic equilibrium. Besides catalysis,
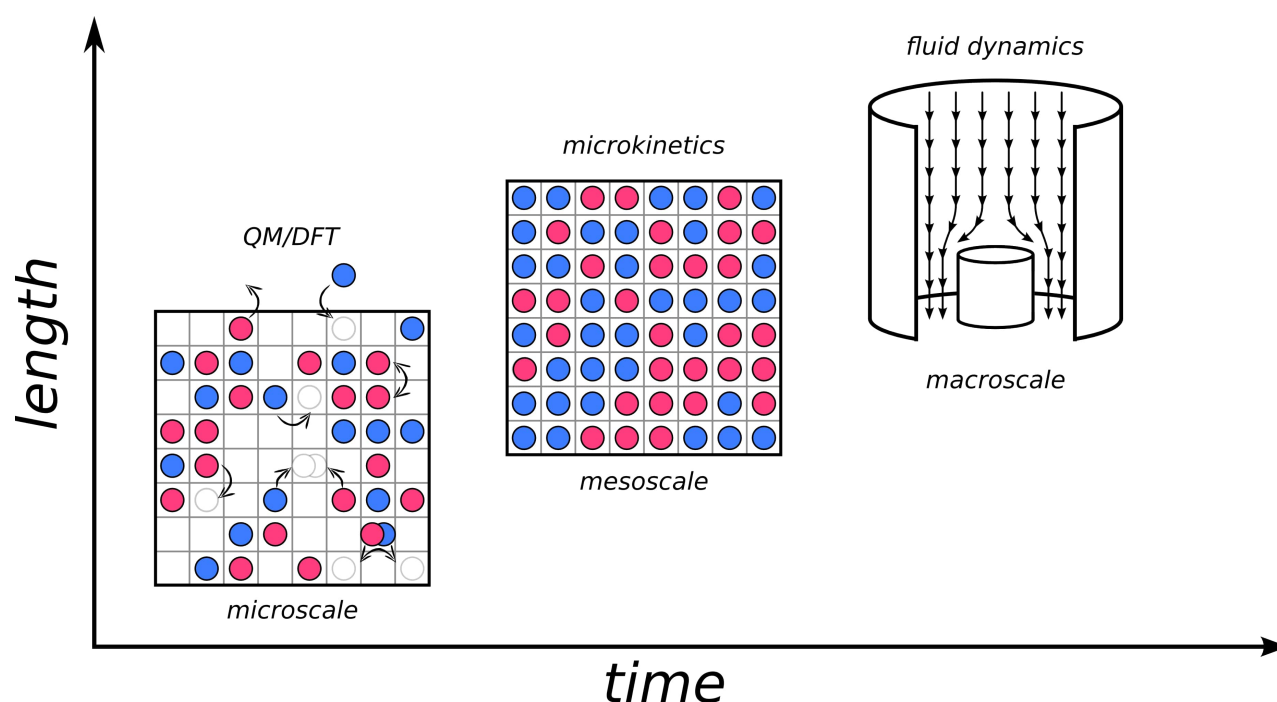
Figure 1. Diagram of three scales involved in a hierarchical multiscale approach to heterogeneous catalysis and the corresponding models and methods. Bottom left: microscale ($\sim$nm in length, $\sim$ns in time). The schematic top view of a catalyst surface shows elementary processes like adsorption and desorption of chemical species, diffusion or reactive events in form of pictorial sketches involving the motion of spheres on a square lattice of active sites. Center: mesoscale ($\sim\mu$m in length, $\sim$ms in time). Microkinetic simulations evaluate the interplay of all the elementary processes on the microscale to yield information on surface composition (illustrated by the shown coverage of the catalyst surface with surface species) and intrinsic catalytic activity. Top right: macroscale ($\sim$m in length, $\sim$minutes/hours in time). Illustration of the fluid flow in a stagnation point reactor where the intrinsic catalytic activity determined by the microkinetic model enters as a boundary condition at all finite element cells describing the catalyst surface.

75 notable such application areas with a similar focus on surfaces or interfaces are diffusion and crystal
76 growth. In this understanding of the use of KMC simulations we will concentrate in the following on
77 this particular technique in these particular application areas. The present is, however, not intended as
78 yet another extensive account of the fundamental methodology. For this we refer the reader to the many
79 excellent reviews available in literature Voter (2007); Chatterjee and Vlachos (2007); Reuter (2011);
80 Stamatakis and Vlachos (2012); Stamatakis (2014). Instead, what we want to provide is a practical guide
81 of how to carry out such simulations (especially in the context of surface kMC), with particular emphasis
82 on best practice recommendations as well as a discussion of current challenges and perspectives.

2 KMC SIMULATIONS: FROM THEORY TO CODES

2.1 Rare-event dynamics: a bottleneck which enables its own solution

84 Many elementary processes involved at surfaces of solids exhibit high activation barriers (even despite
85 a possible reduction of the barrier due to the presence of the catalyst in heterogeneous catalysis). These
86 barriers are usually much larger than k_BT and the corresponding processes are thus classified as rare events,
87 if only thermal energy is there to drive them. While the motion of individual atoms (*e.g.* their vibrations, but
88 also the actual reaction events, *i.e.* crossing an activation barrier once the system has reached the transition
89 state) occurs on picosecond time scales, the time between consecutive high-barrier events can therefore
90 be many orders of magnitude longer, possibly requiring simulations up to seconds or more in order to
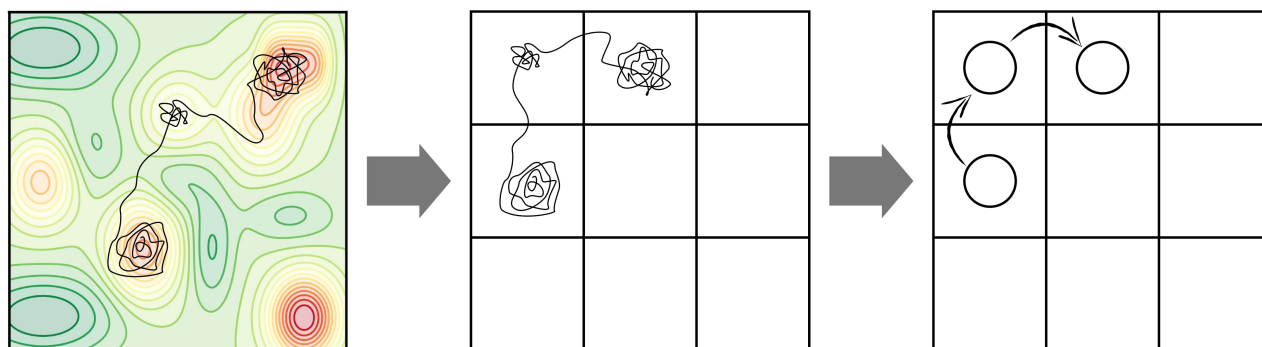
Figure 2. Coarse-graining of a molecular dynamics (MD) trajectory into a Markov chain. Left: a possible MD trajectory (black) overlayed on the underlying potential energy surface (PES) of the system with red regions representing lower-energy basins. A large fraction of time is spent in these PES basins in vibrational motion around the respective minimum. At a certain moment in time, the systems finds an escape route to the next basin. Center: Coarse-graining of PES minima into positions on a suitably defined lattice. Each lattice position represents the basin of attraction of a PES miminum. Right: Coarse-graining of the continuous MD trajectory into a Markov chain of discrete hops between the basins/lattice positions.

91   arrive at meaningful conclusions about the effect of the statistical interplay within an ensemble of multiple
92   possible elementary processes. The "life" of our system in the long time span between these rare events
93   is filled with vibrational motion around a single minimum on the PES. The relevant transitions to other
94   (meta)stable states aka PES basins occur only occasionally. On a mesoscopic time scale, the time evolution
95   of our system therefore manifests itself as a series of consecutive jumps from state to state (see Fig. 2).
96   Additionally, it is intuitive to assume that the longer the time the system spends in one basin, the more
97   it "forgets" how it actually got there. After a while, each possible way to escape from the basin therefore
98   becomes completely independent of the entire preceding history before entering the basin. In other words,
99   the state-to-state jumps of the system constitute a so-called Markov chain (*cf. e.g.* van Kampen (2007)).

100   In consequence, the change of the probability $P_i(t)$ of the system to actually be in state i at time t
101   depends only on the probabilities of hopping out of the current state i into any other state j, k_{ij}, and on the
102   probabilities of hopping into state i from any other state j, k_{ji}. In the present context of chemical kinetics,
103   these hopping probabilities are expressed as rate constants of the elementary processes with units time^{-1}.
104   The overall change in $P_i(t)$ is thus governed by a simple balancing equation, called a Markovian master
105   equation, that only contains these rate constants:

$$\frac{\mathrm{d}P_i(t)}{dt} = -\sum_{j \neq i} k_{ij} P_i(t) + \sum_{j \neq i} k_{ji} P_j(t) \quad . \tag{1}$$

106   From a mathematical standpoint, Eq. 1 is a system of coupled differential rate equations. Seemingly simple,
107   it unfortunately becomes quickly unfeasible to solve explicitly for the number of possible states typically
108   involved in surface catalysis (or diffusion or growth). For a rough estimate, let us consider a system with 100
109   surface sites (*e.g.* an fcc(100) slab of ten atoms per edge in an otherwise periodic boundary condition cell
110   to simulate an extended surface). In the course of a KMC simulation modeling a simple catalytic reaction
111   A + B → AB, each of these sites can assume 3 possible occupation states; it can be empty, occupied by
112   species A or occupied by species B (assuming that a formed product AB immediately desorbs into the gas
113   phase). Already the number of possible configurations of such a trivial toy system is then 3^{100}! The matrix
114   k_{ij} containing all the possible rate constants between system states will thus have $(3^{100})^2 \approx 2.66 \, 10^{95}$

115 elements, making even its comprehensive storage impossible, let alone its diagonalization – and even
116 considering that the limited number of accessible states renders it largely sparse.

117   As an ingenious way out of this mess, the practical Monte Carlo type idea behind KMC is to never
118 even attempt to deal with the entire matrix, but instead to generate stochastic trajectories that propagate
119 the system from state to state (*i.e.* a Markovian sequence of discrete hops to random states happening
120 at random times). From this, the correct time evolution of the probabilities $P_i(t)$ is then obtained by
121 ensemble averaging over these trajectories, or, if the system is in a steady state and ergodicity is ensured, by
122 time averaging over a singular, sufficiently long trajectory. The KMC method thus replaces the analytical
123 solution of Eq. 1 with a numerical approach based on stochastic dynamics. The "only" thing that is needed
124 to make this work is an algorithm that generates suitable such trajectories that (once ensemble or time
125 averaged) yield the correct probabilities $P_i(t)$. This algorithm hence needs to determine at each step along
126 such a state-to-state trajectory to which state the system should jump next and after what time step this next
127 jump should happen. The KMC algorithm does so by selecting elementary processes according to their
128 rate constants, followed by an updating of the time. We will come back to these algorithmic details in Sec. 3.

2.2 Mapping the problem onto a lattice

131   The challenges in applying KMC in practice are largely connected to the plethora of minima on the
132 relevant PESs, and more so, the even larger number of elementary processes connecting them Margraf
133 and Reuter (2019). In the initially sketched multiscale view it would be desirable to employ rate constants
134 calculated from first principles for all of these processes in order to establish models of predictive power.
135 If one considers that each rate constant calculation requires in principle the determination of a transition
136 state to get the activation barrier (*vide infra*), a brute-force KMC approach that requires at each step of a
137 KMC trajectory a large number of such first-principles rate constants is at present and for the foreseeable
138 future in general not feasible. There are currently a number of routes pursued to overcome this showstopper.
139 One obvious remedy would be to recycle first-principles rate constants that have already been computed
140 at previous KMC trajectory steps and thus build up an increasing database. In practice, this requires an
141 unambiguous recognition scheme though that allows to identify that elementary processes that are possible
142 at the present KMC step are identical to processes that were possible in previous steps. Another possibility
143 is to make the rate constant calculations less demanding. This could either be done by resorting to lower
144 levels of theory like using appropriate interatomic potentials instead of DFT or by using more approximate
145 activation barriers *e.g.* from Brønsted-Evans-Polanyi relationships (*vide infra*) that circumvent the costly
146 determination of the transition state. The crucial issue here is always whether then sufficient accuracy is
147 retained to maintain the desired predictive power. This applies most prominently to surface catalysis, where
148 activity and even worse selectivity are highly sensitive to small changes in activation barriers. Finally,
149 one could consider only selective parts of all possible elementary processes, for instance in catalysis by
150 focusing on certain reaction mechanisms only. If such considerations are based on reliable insight (*e.g.*
151 from experimental evidence or other simulations), this can be very elegant. The grain of salt here is that
152 KMC simulations are often employed precisely to find out which of all possible elementary processes
153 crucially govern the statistical interplay. In other words, the objective of KMC is to identify the important
154 parts of process space rather than to assume them in the first place.

155   In this situation, a prevalent school of KMC implementations resolves the problem by exploiting a
156 crystalline order in the studied system. Under such order, it is possible to map the relevant PES minima
157 onto some suitable form of periodic lattice. Different system states, for instance in a surface catalysis
158 KMC simulation, differ then only in their distribution of adsorbates on the various lattice positions. This
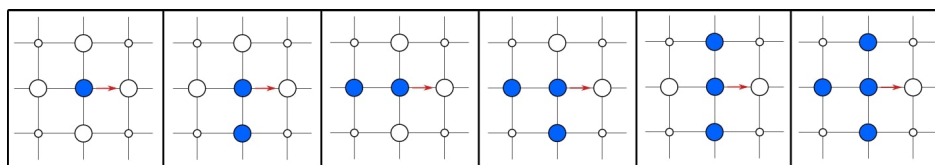
Figure 3. Hopping diffusion process (red arrow) of a particle on a quadratic lattice for all possible configurations of the nearest neighbor lattice sites in the initial state. Configurations that are identical by symmetry are shown only once. The site where the particle diffuses to must be empty for the process to be possible.

159 type of KMC is referred to as *lattice* KMC. Let us illustrate the idea with the simple example of a surface
160 process such as the diffusion of an adatom on an fcc(100) surface. If the stable PES minima correspond to
161 the fourfold hollow sites, we can immediately establish a lattice model where we include only diffusion
162 processes that allow the adatom to start and end up in one of the (hollow) lattice sites. For each state of the
163 system it is usually necessary to relax the geometric structure, and the atoms may not be exactly on the
164 lattice positions after that. However, one has to choose the lattice in such a way so that atoms at least end
165 up close enough to the lattice positions in order to allow for an unambiguous assignment to one lattice site.
166 This already significantly reduces (and ensures the finiteness of) the number of possible processes, which
167 however remains rather large.

168   Further reduction of the number of required rate constants can be achieved by exploiting the translational
169 symmetry of a crystalline lattice. Let us first assume that in our diffusion toy system there is only one
170 single adatom. The translational symmetry of the crystalline lattice then tells that the elementary processes
171 out of any hollow site are all the same. Once we have computed the rate constants for these processes once,
172 we can simply reuse them for the elementary processes out of another hollow site. They will be the same.
173 In the example of our toy system and if we assume that hopping diffusion over a bridge site is the only
174 diffusion mechanism possible, then this means that we have to simply compute just one single rate constant
175 (for such a bridge hopping process). Here, the symmetry refers to the symmetry of the lattice positions
176 *per se*, since (remember) we considered only one adatom in our toy diffusion example. If we have other
177 species occupying nearby lattice positions, this symmetry will readily be broken. What helps in this case is
178 the nearsightedness of chemical interactions as formulated by Walter Kohn. The interaction to some nearby
179 species on the lattice may thus already be so small, that it has a negligible influence on the rate constant. If
180 we neglect such influences between neighboring species to an increasing degree, we restore a complete
181 locality of the elementary processes to the level that we have an as simple and high-symmetry situation as
182 we had in the case of the isolated adatom. For this particular example, the most local approximation would
183 for instance be to completely neglect any interaction with nearby other species – except for preventing
184 diffusion processes in which an adatom would end up in an already occupied site (so-called site blocking).
185 Despite the enormous number of possible configurations of a system with an arbitrary number of adatoms
186 on the lattice, still only one single rate constant for hopping processes over bridge sites would be required.
187 If we consider a (10×10) lattice, then the state-to-state matrix k_{ij} in Eq. (1) is still of the order 2^{100}.
188 However, it only contains elements that are either zero or have this single rate constant as their value. More
189 generally, translational (and maybe any rotational) symmetry does thus not reduce the state space. However,
190 it can dramatically reduce the number of inequivalent rate constants that need to be computed.

191   As a less drastic approximation we may consider only the lateral interactions of the adsorbate with
192 species in nearest neighbor sites. As illustrated in Fig. 3 in our simple diffusion example we will then need
193 to compute five distinct rate constants, one for each possible occupation of the four nearest neighboring

194   sites: one with no nearest neighbors, two with one neighboring site occupied, one with two and and one
195   with three neighboring sites occupied. The generalization to different lattices is a straightforward exercise.
196   Augmenting the local environment that would affect the rate constants would improve the accuracy of
197   the simulation (if such further reaching lateral interactions are indeed still non-negligible), but obviously
198   requires even more rate constant computations. In practice, this gradual inclusion of lateral interactions on
199   a lattice proceeds through cluster-expansion techniques, which we will further discuss in Sec. 9. Essentially,
200   cluster expansions then allow to modify the fundamental rate constant of a given elementary process in the
201   absence of other species to the rate constant of the same process with any distribution of nearby neighbors.

202   In the lattice approximation one can therefore scan all possible configurations and transitions, compute
203   the associated rate constants for any local configuration beforehand and save the latter in a so-called *rate*
204   *catalog*. During the KMC run, the current configuration at a trajectory step is examined and the possible
205   processes and their rate constants are extracted from the rate catalog. An alternative is to identify the
206   possible processes and calculate the cluster-expansion correction to the fundamental process rate constants
207   only *on-the-fly* at each KMC step. This can be numerically more efficient when many lateral interactions
208   are taken into account, and the size and cost of searching a comprehensive rate catalog becomes intractable.
209   Examples of this will be provided in Sec. 9.

210   The approximations used so far can be extremely efficient and may allow for the possibility of using
211   very large supercells in the performed simulations. However, detailed PES information is required and an
212   ordered lattice is assumed as the structural motif. If the lattice model is not suitably chosen, it may neglect
213   important minima of the PES. Simultaneously, any changes of the lattice induced by the simulated dynami-
214   cal processes cannot be captured by construction Reuter (2016). This includes important aspects such as
215   reaction-induced surface reconstruction, other surface morphological transitions or loading-induced lattice
216   transformations in intercalation diffusion. The purpose of *off-lattice* KMC is precisely to overcome such
217   limitations and we will discuss in Sec. 5 how the number of rate constant calculations can then be dealt with.
218

219   ## 2.3   Mean-field approximation

220   An alternative to the full numerical solution of the Master equation (Eq. 1) with KMC is to introduce
221   further approximations (on top of the lattice approximation) that make the equation easier to solve or allow
222   even for an analytical solution. The most common of such approaches is the mean-field approximation
223   (MFA), where the detailed spatial resolution over the extended lattice is sacrificed and replaced by the
224   mean coverage of each considered species at any of the site types exhibited by the lattice. Mathematically
225   speaking, the MFA assumes that the occupation of the different sites on the lattice is statistically independent,
226   *i.e.* that there are no correlations between different sites on the lattice. In the context of surface adlayers,
227   one says that the adlayer is well mixed.

228   Let us begin from the (time-dependent) rate $r_{ij}(t)$ of an elementary process, which is given by

$$r_{ij}(t) = P_i(t)k_{ij} \quad . \tag{2}$$

229   For a start, let us consider only first- and second-order processes, *i.e.* we assume that at most two lattice
230   sites are involved in the elementary process. Per definition, first-order processes do not involve more
231   than one lattice site, *i.e.* the assumption of uncorrelated lattice sites holds trivially. As an example of a
232   second-order process, let us consider the reaction of two neighboring species A and B. We will denote the
233   (time-dependent) pair-probability of finding species A at site a and species B at a neighboring site b with
234    $P_{ab}(A, B, t)$. In the absence of correlations, and assuming that the distribution of the species on the lattice

235   is thus spatially homogeneous, we can write this pair probability as a simple product

$$P_{ab}(A, B, t) = \Theta_a(A, t)\Theta_b(B, t) \quad , \tag{3}$$

236   where $\Theta_a(A, t)$ and $\Theta_b(B, t)$ are the (time-dependent) spatially averaged coverages of species A at sites
237   of type a and species B at sites of type b, respectively. Generalizing this to any reaction order, the MFA
238   hereby condenses the high-dimensional Master equation into much simpler rate equations of the form

$$r_{ij}(t) = N_{ij}k_{ij}\prod_{a \in i}\Theta_a(A, t) \quad , \tag{4}$$

239   where N_{ij} is a geometrical factor accounting for the connectivity of the sites involved in the initial and
240   final states i and j and the species A occupies the site a in the initial state i Matera et al. (2011).

241   The MFA thus yields a set of coupled differential equations, which are solvable by standard algo-
242   rithms Medford et al. (2015). In catalysis, this is often combined with certain assumptions about the
243   rate-determining step (see Sec. 7) to arrive even at an analytical solution for the reaction rate. While
244   these approximations and the MFA approximation itself simplify the problem at hand enormously, one
245   should always keep in mind that they do represent approximations. In particular the MFA is in general
246   only fulfilled for infinitely fast diffusion and in the complete absence of lateral interactions. We will come
247   back to this point in Sec. 8. The first-principles input required for a MFA model is largely the same as
248   for a KMC model, that is, all possible processes and their associated rate constants. However, due to the
249   assumption of (infinitely) fast diffusion inherent to the MFA model, kinetic barriers for diffusion between
250   sites of identical type do not need to be explicitly calculated.
251
2.4   Codes

253   Even though in particular in the context of surface catalysis MFA microkinetic models are still prevalent,
254   one can clearly discern a trend toward KMC simulations. In one way or the other, it is often said that
255   the maturity of a new simulation technique can be judged by the emergence of general-purpose software
256   packages that are user friendly (maybe even up to providing a graphical user interface). If one takes the
257   latter argument at face value, KMC has indeed matured dramatically in the last couple of years. A number
258   of high-end KMC codes have appeared in an astonishingly short period of time. Referring for a more
259   detailed (and maybe exhaustive) account of such codes to the review by Stamatakis *et al.* Stamatakis (2014),
260   we here compile only a brief presentation of a number of such codes to provide an impression of what is
261   presently available:

262   One of the first general-purpose KMC implementations was provided by Lukkien *et al.* in the code
263   `CARLOS` Gelten et al. (1998). In `CARLOS` one can specify any kind of reaction as input, then the program
264   uses pattern recognition to identify possible reactions. `CARLOS` also implements time-dependent rate
265   constants.

266   `SPPARKS`, developed by Plimpton *et al.* Slepoy et al. (2008), implements several KMC solvers and is
267   structured modularly to facilitate expansion and implementation of new models and solvers. Currently
268   implemented models include both lattice and off-lattice applications, as well as a general purpose model
269   for the simulation of biochemical reaction networks.

270   Stamatakis and Vlachos Stamatakis and Vlachos (2011) developed an approach that employs graph-
271   theoretical ideas to overcome the limiting assumption that each participating species occupies a single

272 site and that elementary events involve a maximum of two sites. Here, lattice structure and elementary
273 events are represented as graphs, and lattice processes are identified by solving subgraph isomorphism
274 problems during the simulation. Building on the latter code, Nielsen, Stamatakis *et al.* Nielsen et al. (2013)
275 developed ZACROS, which incorporates cluster expansion Hamiltonians in order to accurately account
276 for long-range lateral interactions. The latter two approaches are suitable for treating systems with rather
277 complex surface chemistry, including organic adlayers and more generally situations where the reactants
278 may adsorb on the surface on multiple sites.

279 The recently developed MonteCoffee Jørgensen and Grönbeck (2018) exploits similar ideas to the
280 graph-theoretical approach, geared towards the simulation of nanoparticles. The code uses neighbor lists
281 to represent the site connectivity, rather than mapping the problem onto a lattice. With respect to the
282 graph-theoretical approaches, hereby the user directly controls the site connectivity.

283 Adaptive KMC (aKMC) approaches (*vide infra*) were mostly developed by Henkelmann and coworkers
284 Henkelman and Jónsson (2001); Xu and Henkelman (2008). The code EON currently includes a set of
285 algorithms to model mesoscale dynamics (parallel replica dynamics, hyperdyamics, and basin hopping as
286 well as aKMC). For aKMC, the code implements a server-client architecture where the client processes are
287 responsible for saddle point searches (see Sec. 4) to escape the current basin, then report the calculated
288 rates back to the server which executes the KMC algorithm.

289 kmos Hoffmann et al. (2014) is an application programming interface based KMC framework that
290 facilitates the generation of an abstract model definition in Python, which is then used to automatically
291 generate efficient Fortran code. The code was instigated by Max Hoffmann and is mainly being developed
292 in our group. We will use it for the hands-on examples in the later sections, providing a detailed practical
293 account on how to run KMC simulations. In the following section we will further describe the KMC
294 algorithm underlying kmos as one example of present-day codes, while in general we emphasize that
295 different codes may implement different algorithms to solve the Master equation.

3 GETTING PRACTICAL: ALGORITHMS AND INPUT DATA

296 As discussed above, the real trick of KMC is the KMC algorithm that generates stochastic trajectories in
297 such a way that their appropriate averaging yields the time evolution of the probability $P_i(t)$ in the Master
298 Eq. (1). One of the most commonly used such KMC algorithm, initially developed by Bortz, Kalos and
299 Lebowitz Bortz et al. (1975) for Ising spin systems, is known as the BKL algorithm (after the authors)
300 or the "n-fold way". It also goes under the names of Variable Step Size Method Jansen (1995) or Direct
301 Method Gillespie (1976). For a simple, practical rationalization of the algorithm, let us consider a toy
302 system which can assume only two states A and B connected by a barrier with associated rate constants
303 k_{AB} and k_{BA} for the forward and backward transitions, respectively. In this system, only two elementary
304 events are possible; if, say, the system is sitting in state A, it can hop to state B. As the rate constant for
305 this hop is k_{AB} (with unit time^{-1}), one may naively think that the average time that will have passed until
306 such a hop occurs is $\Delta t_{AB} = k_{AB}^{-1}$. Obviously for the hop back from state B to state A, the average time
307 would be $\Delta t_{BA} = k_{BA}^{-1}$. Accordingly, a KMC algorithm would generate a trajectory where after each hop
308 the time is incremented by Δt_{AB} or Δt_{BA} (depending on what hop occurred).

309 Mathematically, this naive thinking is not entirely correct. In reality, while being in state A for each short
310 increment of time the system will have the same probability of finding the escape path. This generates an
311 exponentially decaying survival statistics, whose derivative represents the probability distribution p_{AB} for
312 the true time of first escape:

$$p_{AB}(t) = k_{AB} \exp(-k_{AB}t) \quad . \tag{5}$$

313 The average escape time thus has to be appropriately weighted by this Poisson distribution. It can be shown
314 Gillespie (1976); Fichthorn and Weinberg (1991) that this is achieved by advancing the system clock by

$$\Delta t_{AB} = -\frac{\ln(\rho_2)}{k_{AB}} \quad , \tag{6}$$

315 where $\rho_2 \in]0,1]$ is a randomly drawn number.

316 When we now generalize this to an arbitrary system, where at each step along a KMC trajectory a
317 multitude of processes $i \to j$ from the current state i to other states j are possible, the theory of Poisson
318 processes allows to straightforwardly derive the average time that will have passed until *any* process has
319 occurred. Since the elementary processes are independent, each has its own probability distribution p_{ij}
320 given by

$$p_{ij}(t) = k_{ij} \exp(-k_{ij}t) \quad , \tag{7}$$

321 and the probability of the time of first escape from state i through *any* of the processes $i \to j$ follows as

$$p_{\text{escape}}(t) = k_{\text{tot}} \exp(-k_{\text{tot}}t) \quad , \tag{8}$$

322 where

$$k_{\text{tot}} = \sum_j k_{ij} \tag{9}$$

323 is the total escape rate constant obtained as the sum of all the individual elementary rate constants. Just as
324 for the single process case, the average escape time is then

$$\Delta t_{\text{escape}} = -\frac{\ln(\rho_2)}{k_{\text{tot}}} \quad , \tag{10}$$

325 where $\rho_2 \in]0,1]$ is a randomly drawn number. It is crucial to highlight that this escape time only depends on
326 the total rate constant, and is independent of the actual process that actually occurs to bring the system out
327 of the current state i. This actual process nevertheless needs to be identified, since this is what determines
328 to which state j the system propagates. This state j is then the starting point for the next KMC step, *i.e.* the
329 next KMC step evaluates the escape from this particular state j.

330 The BKL algorithm determines this executed process out of all possible processes again by rolling the
331 dice. Imagine a stack of segments of height proportional to the rate constants k_{ij} of the possible processes,
332 which correspondingly sums up to a total height of k_{tot}. We can choose a process to execute out of this
333 stack by drawing a random number ρ_1 and multiplying it by k_{tot}. The resulting number will "point" at the
334 process with correct probability in the process stack, as illustrated in Fig. 4. The selected process is then
335 executed, bringing our system into a different state for the next KMC step. This way of choosing out of the
336 stack ensures that faster processes are selected with a higher probability than slower ones: They have a
337 larger rate constant, have correspondingly a thicker segment in the stack and are correspondingly chosen
338 more often. We therefore have a recipe to generate trajectories that satisfy the Master equation, obtained
339 stochastically via the extraction of only two random numbers $\rho_1, \rho_2 \in]0,1]$. An important parameter is
340 thereby also the random number seed used to generate the sequence of random numbers, as recalculating
341 the trajectory with a new seed value will lead to the new trajectory that is statistically independent of the
342 former.

343 The algorithm, also illustrated in Fig. 4, may thus be summarized as follows:
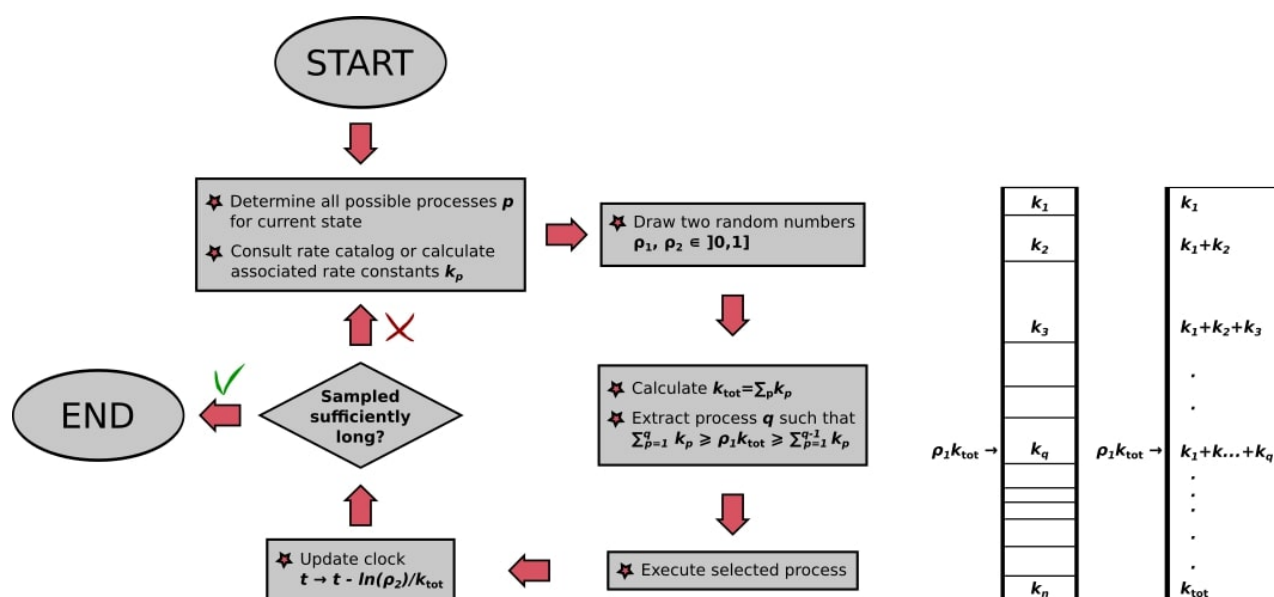
Figure 4. Left: Flowchart of the BKL algorithm as implemented in kmos. Right: Graphical illustration of random process selection in the process stack.

344   • Make a list of possible processes p for the system to escape the current state i, with associated rate
345   constants k_p;

346   • draw two random numbers $\rho_1, \rho_2 \in]0, 1]$;

347   • calculate $k_{\mathrm{tot}} = \sum_p k_p$;

348   • extract process q, which has to fulfill the constraint $\sum_{p=1}^{q} k_p \geqslant \rho_1 k_{\mathrm{tot}} \geqslant \sum_{p=1}^{q-1} k_p$;

349   • execute randomly drawn process;

350   • update clock: $t \to t - \ln(\rho_2)/k_{\mathrm{tot}}$.

4 RATE CONSTANTS FROM FIRST PRINCIPLES: TRANSITION STATE THEORY

351 As discussed in the previous sections, KMC requires rate constants for all considered elementary processes
352 as an input. For the surface applications focused on here, these rate constants are at present predominantly
353 obtained through Transition State Theory (TST). Making a number of assumptions, for instance that the
354 flux of trajectories passing the transition state (TS) from state i to j will never come back to the state i
355 (no-recrossing rule) and that the barrier crossing is a purely classical event (no tunneling), TST provides a
356 simple expression for the rate constant, known as Eyring (or Eyring-Polanyi) equation: Laidler (1987)

$$k_{ij}^{\mathrm{TST}} = \frac{q_{\mathrm{TS}}^{\mathrm{vib}}}{q_i^{\mathrm{vib}}} \frac{k_{\mathrm{B}}T}{h} \exp\left(-\frac{\Delta E_{ij}}{k_{\mathrm{B}}T}\right) = k_o \frac{k_{\mathrm{B}}T}{h} \exp\left(-\frac{\Delta E_{ij}}{k_{\mathrm{B}}T}\right) \quad, \tag{11}$$

357 where T is the absolute temperature, h is Planck's constant, $q_{\mathrm{TS}}^{\mathrm{vib}}$ and q_i^{vib} are the partition functions at the
358 transition state and at the initial state, respectively, and ΔE_{ij} is the activation barrier of the process. The
359 latter is directly available from PES information and therefore accessible to first-principles calculation
360 (*e.g.* semi-local DFT). The prefactor $k_o \frac{k_{\mathrm{B}}T}{h}$ may in principle be calculated. Most popular is harmonic
361 TST, where the partition functions are obtained from the vibrational modes at the initial state i and at
362 the TS. In the predominant number of studies the considerable computational costs of these vibrational
363 calculations are avoided though, and one simply approximates $k_o \simeq 1 - 10$, yielding a prefactor in the
364 range $10^{12} - 10^{13}\,\mathrm{s}^{-1}$. This is never really fully justified, and if at all only when the vibrational properties
365 of the TS do not differ much from those of the initial state. A prominent class of processes where this
366 common approximation is not valid are non-activated adsorption processes, where the prefactor needs to
367 account for the strong entropy reduction from the gas phase to the surface-bound state. In this case the rate
368 constant is better estimated as: Reuter and Scheffler (2006); Chorkendorff and Niemantsverdriet (2017)

$$k_{n,B}^{\mathrm{ads}}(T, p_n) = \widetilde{S}_{n,B}(T) \frac{p_n A_{\mathrm{uc}}}{\sqrt{2\pi m_n k_{\mathrm{B}}T}} \quad, \tag{12}$$

369 where p_n is the partial pressure of species n of mass m, and the local sticking coefficient $\widetilde{S}_{n,B}(T)$ governs
370 the fraction of impinging particles sticking to a site B located in a surface unit cell of area A_{uc}.
371

4.1 Master equation and detailed balance

373 We will next motivate some practical guidelines that the input (processes and rate constants) to any
374 microkinetic model (KMC or MFA) must adhere to. Let us consider a system that has reached steady
375 state. This imposes the constraint of vanishing derivative in the Master equation (Eq. 1), which leads to the
376 condition

$$\sum_{j\neq i}\left[k_{ij}P_i^* - k_{ji}P_j^*\right] = 0 \quad, \tag{13}$$

377 where P_i^* (P_j^*) is the time-independent probability that the system is in state i (j). This condition is a
378 conservation law stating that the sum of the rates of all transitions out of any state i (j) must equal the sum
379 of the rates of all transitions into state i (j). At thermodynamic equilibrium, microscopic reversibility and
380 the principle of detailed balance Tolman (1925) imposes the even stronger constraint that the average rate
381 of every microscopic process must exactly balance its reverse process

$$\frac{k_{ij}}{k_{ji}} = \frac{P_j^*}{P_i^*} \quad. \tag{14}$$

382 The right-hand side of Eq. 14 is thereby proportional to the states' Boltzmann weights and can thus be
383 expressed in terms of the free energy difference between states i and j:

$$\frac{k_{ij}}{k_{ji}} = \exp\left(-\frac{F_j(T) - F_i(T)}{k_{\mathrm{B}}T}\right) \quad . \tag{15}$$

384 The above derivation motivates two practical guidelines for constructing KMC (or MFA) models. The
385 first guideline is that every microscopic process must have defined a corresponding reverse process, and
386 the second guideline is that the rate constant expressions used for the forward and reverse processes must
387 fulfill Eq. 15.

388 For the latter point it is particularly crucial to realize that this also extends to computing the free energies
389 of both states F_i and F_j with the same numerical approximations. In practice, this is often neglected
390 (different supercells/configurations, mix of first-principles and empirical data etc.) and can then have drastic
391 consequences as the kinetic model is not thermodynamically consistent Mhadeshwar et al. (2003); Schmitz
392 (2000). Quite some work has therefore been devoted to achieve an overall thermodynamic consistency, *e.g.*
393 Mhadeshwar et al. (2003); Nielsen et al. (2013).

394
395 ## 4.2 Obtaining rate constants: Transition state search

396 In the context of determining rate constants, it is natural to put a primary focus on the *lowest* activation
397 barriers that need to be overcome, *e.g.* in catalysis on the *minimum energy path* connecting reactants and
398 products. From the mathematical standpoint, locating the lowest barrier(s) translates into locating the
399 lowest first-order saddle point(s) on the PES, which is a particularly challenging task for which – in contrast
400 to locating PES minima – there is yet no general approach that is guaranteed to work. In the following
401 we will briefly discuss the reliability, accuracy and performance of different available methods. Always
402 keeping in mind that "your mileage may vary", there is nevertheless a general guideline as to which family
403 of approaches would be preferable depending on the nature of the problem at hand. For lattice KMC one
404 would assume or derive the mechanism (*e.g.* the reaction mechanism in the context of heterogeneous
405 catalysis) and subsequently compile a list of the elementary processes that constitute this mechanism. In
406 this case, initial and final states are therefore pre-determined, enabling the use of so-called *interpolation*
407 methods. For adaptive KMC, more often than not no previous assumption of mechanism is made and one
408 may need to blindly explore the possible and most probable escape pathways from a current state. So-called
409 *local* methods are then mandatory, as only information on the initial state is available.

410
411 ### 4.2.1 Interpolation methods

412 The simplest form of interpolation-based TS search consists in identifying a reaction coordinate guess in
413 one or a small number of internal degrees of freedom, preferring those that describe the main structural
414 differences between initial and final state. The selected coordinates are subsequently constrained to specific
415 values between the initial and final structures, while all remaining degrees of freedom are optimized. Such
416 TS searches are often referred to as *coordinate-driving* (*drag*) methods Halgren and Lipscomb (1977);
417 Rothman and Lohr (1980); Williams and Maggiora (1982). The success of drag methods depends critically
418 on the ability to choose a good set of reaction coordinates and on the topology of the PES in the direction
419 of the remaining degrees of freedom. In general, if the reaction path is dominated by only one or two
420 degrees of freedom, the coordinate driving may work, and the constrained optimized geometry (with the
421 smallest residual gradient) is a good approximation to the TS. On the other hand, a bad choice of reaction

422 variable(s) may lead to hysteresis and converge to (unphysical) discontinuous reaction paths Halgren and
423 Lipscomb (1977); Henkelman et al. (2002).

424 Drag methods operate on one structure at the time. A significant improvement is achieved by simulta-
425 neously optimizing multiple points along the initial guess of the reaction path. An example is the *ridge*
426 method Ionova and Carter (1993), which iteratively refines an initial guess of the TS by simultaneously
427 relaxing two replicas of the latter, sligthly displaced across the ridge of the PES, until they contract to
428 the actual TS. Methods that operate with more than two structures are often referred to as "chain-of-state"
429 methods. The initial distribution of structures will typically be along a linear interpolation of coordinates
430 between the initial and final, or any convenient form of continuous variation along a chosen reaction path.
431 All intermediate states or images are then optimized simultaneously in some concerted way, providing not
432 only the saddle point, but also a good approximation of the entire reaction path.

433 Among those, the *Nudged Elastic Band* (NEB) method Jónsson et al. (1998); Henkelman and Jónsson
434 (2000) is arguably most popular as it incorporates strong points of older approaches in order to cure their
435 shortcomings. After initializing an initial chain of images $\mathbf{R}_i$, NEB minimizes a target function ("elastic
436 band") defined as the sum of energies of all intermediate images and an additional penalty term which
437 distributes the points along the path through a single spring constant k (see Fig. 5):

$$S_{\mathrm{EB}}(\mathbf{R}_1, \ldots, \mathbf{R}_N) = \sum_{i=1}^{N} E(\mathbf{R}_i) + \sum_{i=1}^{N-1} \frac{1}{2} k(\mathbf{R}_{i+1} - \mathbf{R}_i)^2 \quad . \tag{16}$$

438 In general, a straightforward minimization of S_{EB} would exhibit a tendency to "cutting corners" if the
439 spring constant k is too large, and "sliding down" towards the extrema if k is too small (thus undersampling
440 the actual TS region). These problems are alleviated by "nudging" the elastic band, *i.e.* by using only the
441 component of the spring force parallel to the tangent of the path (to cure for corner-cutting), and only the
442 perpendicular component of the energy force (to cure for down-sliding). The total force acting on each
443 image is then

$$\mathbf{F}_{i,\mathrm{NEB}} = \mathbf{F}_{i\parallel}^s - \mathbf{F}_{\perp}^i = k \left(|\mathbf{R}_{i+1} - \mathbf{R}_i| - |\mathbf{R}_i - \mathbf{R}_{i-1}| \right) \hat{\tau}_i - \nabla E(\mathbf{R}_i)_{\perp} \quad , \tag{17}$$

444 $\hat{\tau}_i$ being the tangent unit vector at image i. In the Climbing-Image NEB (CI-NEB) Henkelman et al. (2000)
445 variant, the image with the highest energy is selected after a few iterations and driven up towards the saddle
446 point by turning off its spring force and reversing the component of the potential force parallel to the chain.
447 This yields exactly the saddle point (which in the non-climbing version is obtained by interpolation) at no
448 additional computational cost.

449 The NEB method is still likely to run into trouble when dealing with a PES for which the energy varies lar-
450 gely along the reaction path, but very little perpendicular to it. Regarding this problem, it has been pointed
451 out that for CI-NEB corner cutting does not affect the accuracy of the TS, and that a more robust relaxation
452 to the TS may be achieved by using the full spring force rather than only the component parallel to the
453 tangent of the path Kolsbjerg et al. (2016). Furthermore, as all such algorithms in its category, NEB comes
454 at a high computational cost as it involves the optimization of many structures and typically requires a rather
455 large number of iterations. Technical parameters such as the number of images and the value of the spring
456 constant must be wisely chosen beforehand. The latter issue in particular may prove to crucially influence
457 the optimization efficiency: a small value causes an erratic coverage of the reaction path, while a large value
458 focuses the effort on distributing the points rather than on finding the reaction path, and consequently slows
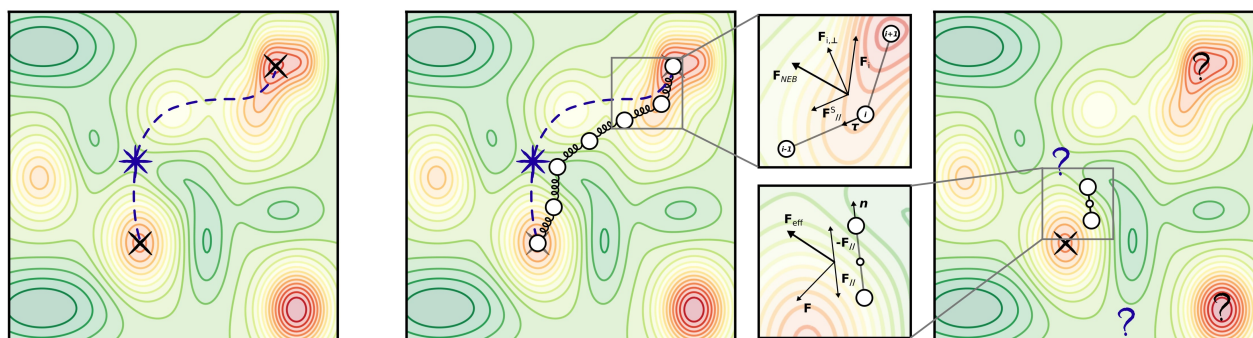
Figure 5. Transition states and most popular transition state (TS) search methods. Left: An arbitrary PES exhibiting multiple minima (indicated by red colors). Black crosses mark two local minima, *e.g.* initial state (IS) and final state (FS) of a known elementary reaction. A violet star marks the location of the TS; a violet dashed line represents the minimum energy path connecting IS and FS. Center: illustration of the NEB method. The magnified panel shows the composition of forces which determines the effective NEB force acting on an image i at a certain optimization step. Right: illustration of the dimer method. The magnified panel shows the composition of forces which determines the effective force acting on the dimer at a certain optimization step, after the constrained minimization with respect to orientation.

459   down the convergence. In the traditional NEB method the number of images are fixed during the simulation
460   and it can be challenging to reach a good compromise between a sufficient coverage of the reaction path
461   and the computational cost. To mitigate this, an automated NEB (AutoNEB) algorithm has been proposed
462   Kolsbjerg et al. (2016), which can save computational resources by focusing first on converging a rough
463   path before improving on the resolution around the TS. An alternative solution to the same problem has
464   been proposed in the truncation-based energy weighting string method Carilli et al. (2015), which uses
465   energy weighting to focus the computational effort on the physically interesting images within the barrier
466   region. Finally, it is also worth mentioning the growing string method (GSM) Peters et al. (2004), which
467   circumvents the need for a (good!) initial guess of the reaction path by separately evolving two string
468   fragments, one associated with the reactants and the other with the products, until the fragments converge
469   and thereby define the reaction path. The combination of GSM with an eigenvector following TS search
470   Zimmerman (2013) has shown promising results for a benchmark set of more than 100 elementary reactions.
471
472   ## 4.2.2   Local methods
473   Keeping in mind that transition states are points where the gradient vanishes, they may in principle be
474   located by minimizing the gradient norm. This is exactly the working concept behind the so-called local
475   methods. In contrast to interpolation methods, local methods only use information of the PES function and
476   its first and possibly also second derivatives at each point, *i.e.* they require *no* knowledge of the initial-state
477   and/or final-state geometries. They do, however, usually require a good estimate of the TS to use as a
478   starting geometry in order to converge. This is one of their main limitations.

479   A most common member of the local group of methods is the Newton-Raphson (NR) approach, which
480   locates the TS directly, given that one starts the search sufficiently close to the TS. Sufficiently close here
481   means already in the harmonic region with the Hessian having exactly one negative eigenvalue. Under
482   these conditions, computing the Hessian and inverting the second order Taylor expansion directly yields
483   the step which maximizes the energy along the TS eigenvector and minimizes the energy along all other
484   directions, converging exactly to the TS. The main drawback of the NR method is the need for generating
485   and manipulating the full Hessian matrix.

486 However, the main function of the Hessian for saddle point optimization is to provide the direction along
487 which the energy should be maximized (lowest ascent if sufficiently near the TS). The dimer method
488 Henkelman and Jónsson (1999) can be employed to determine this direction without calculating the
489 Hessian explicitly, employing two symmetrically displaced replicas–the dimer (see Fig. 5), which is used
490 to transform the force in such a way that optimization leads to convergence at a saddle point rather than at
491 a minimum. In general, the strategy for the dimer method is to try many different initial configurations
492 around a minimum, usually taking them from the extrema of a short high-temperature MD trajectory in
493 order to find the saddle points that lead out of that basin. In a first step, the dimer is minimized with respect
494 to orientation by imposing a constrained distance between the images. The lowest mode direction is then
495 given by the line connecting the two images, and this can be used for displacing the central structure, *i.e.*
496 translating the dimer, which is then followed by a new dimer optimization and so on. The force acting on the
497 centre of the dimer gets modified by inverting the component in the direction of the dimer: minimization of
498 this force drives the dimer to a saddle point. A dimer optimization can be done using only first derivatives,
499 and thus alleviates the need for calculating the Hessian matrix. In general, however, performance scaling
500 with system size is not really known. It is unclear in particular whether the added computational cost
501 of optimizing each dimer configuration eventually outweighs the saving by not requiring an explicit Hessian.
502
4.2.3 BEP and scaling relations
504 An alternative, cheaper approach to determine activation barriers, which still retains grounds in first
505 principles, is provided by the employment of approximate energy relations. The most prominent example is
506 the Brønsted-Evans-Polanyi (BEP) relation Nørskov et al. (2002); Michaelides et al. (2003), which yields
507 linear relationships of the kind

$$\Delta E \simeq c_1(E_{\mathrm{FS}} - E_{\mathrm{IS}}) + c_2 \quad , \tag{18}$$

508 where c_1 and c_2 are constants and E_{FS} and E_{IS} are the total energies of the final and initial states,
509 respectively. The latter are obtainable from local geometry relaxations, and hence significantly cheaper
510 than even the sloppiest TS search. The two parameters c_1 and c_2 need to be determined by linear fitting to
511 appropriate first-principles calculations. The parameters are in general only transferable to site types that
512 are similar to those used in the fitting, *e.g.* the fcc(111) sites of transition metal surfaces, but they can be
513 rather universal among different kinds of reactions Wang et al. (2011).

514 Furthermore, it has been shown that the binding energies of many reactants, products and intermediates
515 at transition metal surfaces correlate with the binding energies of the few base elements (mostly C, N,
516 O, S, halogens) with which the molecules typically bind to the surface Abild-Pedersen et al. (2007). The
517 employment of such scaling relations, combined with BEP relations, enables an enormous reduction of
518 the computational cost of getting first-principles rate constants for applications such as catalyst screening,
519 where a large number of rate constants have to be computed for "similar" processes.

5 GARBAGE IN – GARBAGE OUT

520 As always in modeling, it is important to realize that the predictions made from a model are limited by
521 the quality of the input data to the model, commonly expressed as the *garbage in – garbage out* (GIGO)
522 principle. The necessary input data to a KMC model are the possible processes as well as their associated
523 rate constants. As discussed above, in the context of first-principles KMC simulations where the rate
524 constants are determined by DFT or other electronic structure calculations, these input data are at present
525 typically determined beforehand. In other words, rather than the KMC simulation identifying by itself
526 what processes are important or should be considered and at which accuracy, the simulation depends on a

527 fixed given list of such processes with rate constants that come with the typical uncertainty imposed by
528 the underlying DFT calculation (the rate catalog). This rigid setup leads to a high sensitivity of the KMC
529 simulation results on this input data.

530   As already mentioned initially, advanced KMC approaches that overcome at least some of the limitations
531 of this prevalent rigid input-data setup are a long sought goal and topic of current research. One possibility
532 to automatically identify the relevant processes in a system would be to use (accelerated) MD approaches
533 like hyperdynamics, temperature-accelerated dynamics or replica-exchange dynamics beforehand Voter
534 et al. (2002). In adaptive (on-the-fly) KMC a process search using the dimer method or high-temperature
535 MD simulations is directly integrated into the KMC algorithm Henkelman and Jónsson (2001); Chill and
536 Henkelman (2014). A great advantage of the latter methods is also that the KMC model does not necessarily
537 have to be implemented on a fixed lattice. However, they are generally also much more computationally
538 demanding, as they require many orders of magnitude more energy and force evaluations to determine all
539 processes and their barriers. Applications have therefore been limited to rather simple systems or systems
540 where the energy and force evaluations can be done with classical force fields instead of DFT Xu and
541 Henkelman (2008); Konwar et al. (2011); Pedersen et al. (2015). At least for the time being, first-principles
542 KMC simulations in the application areas covered here are instead in practice only tractable within the
543 rigid setup, which is why we concentrate on it from now on in this practical guide.

544   In the following we will illustrate the above-described concepts using a simple model for the diffusion of
545 Au adatoms on a Au(100) surface. This will highlight possible pitfalls, but will also provide guidance for
546 best practice. All discussed KMC models have been implemented in the `kmos` software package Hoffmann
547 et al. (2014) and are available in the supplemental data.
548
5.1   Adatom diffusion on Au(100)

550   The simplest diffusion process one can think of in this system consists of the hopping of Au atoms
551 between the fourfold hollow adsorption sites offered by the Au(100) surface lattice, see Fig. 6(a). For a
552 simple KMC model of this system we will consider a (20×20) square lattice of adsorption sites. The
553 possible processes are the hops of particles from one site into one of the four neighboring sites up, down,
554 left and right. Neglecting any possible lateral interactions between Au adatoms, the barrier for any of
555 these processes is the same and at the DFT-LDA level it has been calculated to $\Delta E_{\text{diff}} = 0.83\,\text{eV}$ Yu and
556 Scheffler (1997). We will use the TST expression (Eq. 11) to express the rate constant of the diffusion
557 processes in terms of this barrier. For simplicity we will ignore any entropic corrections to the barrier and
558 zero-point vibrational energy corrections, *i.e.* $k_o = 1$. In order to run the KMC model we need to fill some
559 of the lattice sites with particles. If we were to initialize the simulation with an empty lattice, we would
560 directly hit a deadlock where no processes are possible. In this example we prepare the initial state by
561 randomly filling sites with Au adatoms corresponding to a coverage of 0.25 monolayer (ML), *i.e.* every
562 fourth surface site is occupied. As the output of the simulation we calculate the diffusion coefficient of the
563 Au adatoms by tracking the mean squared displacements (MSD) Garhammer (2017) as a function of time.
564 The diffusion coefficient D can then be calculated as

$$D = \frac{\langle \text{MSD}(t) - \text{MSD}_0 \rangle}{2dt} \quad , \tag{19}$$

565 where t is the simulation time and d is the lattice dimension (2 in this case). The averaging $\langle \rangle$ is performed
566 over all Au adatoms. In order to improve the statistics 25 independent simulations were run, which differed
567 from each other in the random initialization of the lattice and in the random number seed used. The pink
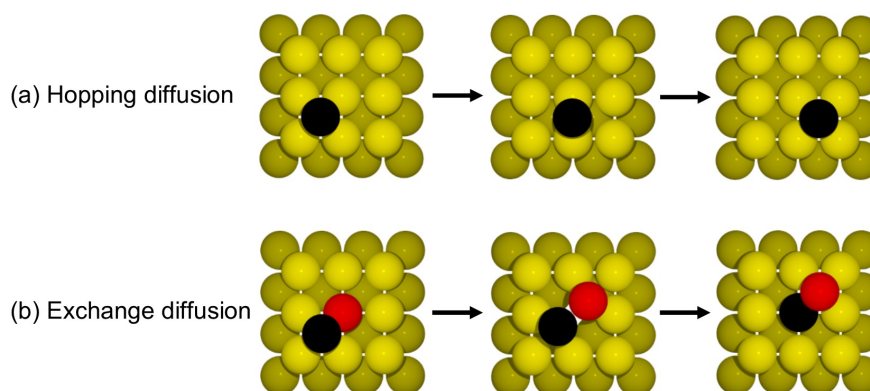
Figure 6. Illustration of the mechanism for (a) hopping and (b) exchange diffusion (see text).
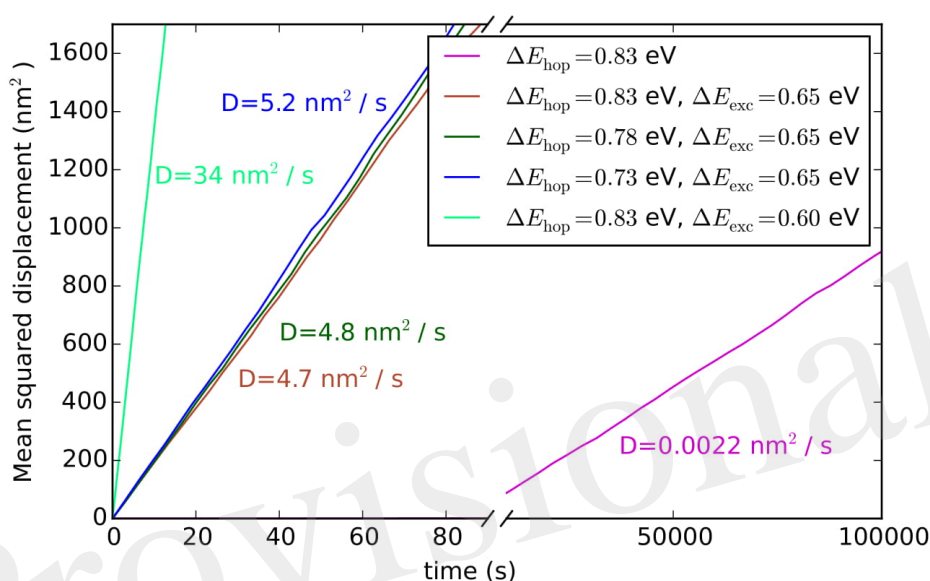

Figure 7. Averaged mean squared displacements and diffusion constants of adatoms on Au(100) for hopping and exchange diffusion processes and various associated barriers.

568 line in Fig. 7 shows the average of these 25 simulations from which the diffusion coefficient is determined
569 to be 0.0022 nm^2/s.

570   Such hopping diffusion processes are, however, not the only mechanism possible for self-diffusion
571 on metal surfaces. Both experimentally and theoretically an alternative exchange diffusion mechanism
572 has been described Bassett and Webber (1978); Wrigley and Ehrlich (1980); Feibelman (1990); Yu and
573 Scheffler (1997), in which a metal adatom replaces a surface layer atom and pushes it to a neighboring
574 adsorption site, see Fig. 6(b). With the adatom and surface atom of the same species, this effectively also
575 results in a net displacement. In Ref. Yu and Scheffler (1997) it was found that this process occurs with the
576 lower barrier of only 0.65 eV on Au(100), and should therefore dominate over hopping diffusion. When
577 we additionally allow for this diffusion process in the model, the output of the simulation changes indeed
578 dramatically, since the barrier enters the rate constant for diffusion exponentially. Including exchange
579 diffusion, the diffusion coefficient is now determined to be 4.7 nm^2/s, see brown line in Fig. 7, *i.e.* more
580 than three orders of magnitude higher than before. It can also be noted that the timescale reached in the
581 simulation (for the same number of total KMC steps) is much shorter with exchange diffusion. In general,

582 the time advanced with a KMC step, $\Delta t_{\mathrm{escape}}$, and therefore the total timescale that is computationally
583 reachable during a simulation, depends on the sum of all rate constants (see Eq. 10), which is dominated by
584 the fastest process in the system.

585   The above example thus highlights the extent to which the outcome of a KMC simulation is dependent
586 on knowing and allowing for all relevant processes in the model. This is a severe limitation and requires
587 utmost caution and care in setting up a KMC model. The likelihood to overlook a non-intuitive process
588 such as exchange diffusion cannot be overemphasized and then - alas - the GIGO principle applies with full
589 might. Another drawback of first-principles KMC is that the DFT energies entering the rate constants can
590 have rather large errors associated with them. For processes at extended surfaces often low-rung semi-local
591 DFT functionals (possibly with some $+U$ correction) are still the state-of-the-art. This means that DFT
592 errors on barriers may easily be on the order of $0.1 - 0.2\,\mathrm{eV}$. Considering that these barriers enter the rate
593 constants exponentially, see Eq. 11, the associated rate constants could be wrong by orders of magnitude.
594 However, in general, errors associated with the various rate constants entering a KMC model do not all
595 have a similar effect on the output of the simulation. To illustrate this, we plot in Fig. 7 the output of the
596 diffusion model including both hopping and exchange diffusion, when lowering the barrier for hopping
597 diffusion by $0.05\,\mathrm{eV}$ (dark green line) and by $0.1\,\mathrm{eV}$ (blue line). As can be seen, the result only begins to
598 change significantly when the barrier for hopping diffusion comes within few tens of meV of the barrier
599 for exchange diffusion. In contrast, lowering the rate constant for the dominant exchange diffusion process
600 by only $0.05\,\mathrm{eV}$ (light green line) leads to a seven times higher diffusion constant. Again, this is a result of
601 the exponential dependence of the rate constant on the barrier. In other words, a DFT error of $0.1\,\mathrm{eV}$ on
602 hopping diffusion would not change the output of the simulation, while the same DFT error on exchange
603 diffusion would lead to huge changes in the output.

604   While this behavior is trivial to guess in this simple two-parameter model, KMC models, particularly
605 in catalysis, can be much more complicated with very many reaction steps and competing pathways. It
606 is then of interest to identify more systematically those processes and their input rate constants that are
607 most important for the outcome of the simulation. Within the more general context of multiscale modeling,
608 viewing first-principles KMC simulations as a hierarchical multiscale modeling setup combining an
609 electronic structure with a mesoscopic statistical technique, such endeavors are called sensitivity analyses.
610 As has hopefully become clear from this simple adatom diffusion model, for the rigid KMC setup such
611 analyses are absolutely pivotal to assess the meaningfulness of the obtained results. In addition, such
612 analyses also provide important insight into which processes are those that control the kinetics, as it is the
613 rate constants of these processes that critically determine the simulation outcome. Such mechanistic insight
614 is another important reason for conducting KMC simulations. In catalysis, these controlling processes are
615 called rate-determining steps, and identifying rather than assuming them for a catalytic cycle is one of
616 the big assets of comprehensive KMC simulations. We will come back to this topic in Sec. 7 after having
617 discussed examples for such more complex catalysis KMC models in the next section.

6   STEADY-STATE AND TRANSIENT SIMULATIONS FOR SURFACE CATALYSIS

618 For catalysis applications one is often interested in the behavior of the system once it has reached steady
619 state (see Eq. 13). Since the system is open (constant influx of reactants, constant outflux of products),
620 this still requires kinetic simulations even though the quantities of interest are *per se* generally not time-
621 dependent. Major such quantities of interest are the surface composition (for instance in form of averaged
622 coverages of different adsorbates/reaction intermediates), reaction mechanisms and production rates of
623 various chemicals. The latter reaction rate is often expressed as a turnover frequency (TOF), which is the
624 average rate of production of a certain molecule per second per surface site (or surface area). Alternatively,
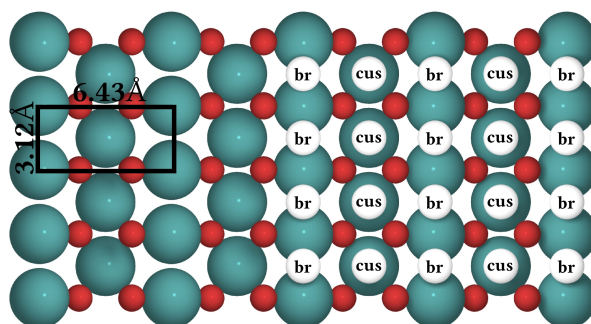
Figure 8. Top view of the structure of the $RuO_2(110)$ surface. To the left, the surface unit cell is shown as a black rectangle. Big green spheres = Ru atoms, small red spheres = O atoms. To the right, the coarse-grained lattice structure is sketched. It consists of alternating columns of cus (coordinately unsaturated) and br (bridge) sites.

625 for analysis methods like temperature programmed reaction Jansen (1995); Rieger et al. (2008), cyclic
626 voltammetry Rai et al. (2006) or titration Piccinin and Stamatakis (2014) one might be interested in the
627 transient behavior of a system prepared in a given initial state. In the next section we will introduce a
628 simple catalysis KMC model for CO oxidation on $RuO_2(110)$ and illustrate the preparation of various
629 initial states and possible pitfalls with the relaxation to the steady-state solution.
630

6.1   CO oxidation on $RuO_2(110)$

632   The CO oxidation model is taken from Ref. Reuter et al. (2004) and we refer to this publication for its
633 more detailed motivation. In this model, the $RuO_2(110)$ surface is considered to contain two types of active
634 sites, br (bridge) and cus (coordinately unsaturated) sites, arranged in an alternating rectangular lattice as
635 shown in Fig. 8. Each site can be either empty or occupied by O or CO. A total of 26 processes are possible
636 in this system, covering non-dissociative CO adsorption/desorption, dissociative O_2 adsorption/desorption,
637 diffusion of O and CO, as well as CO_2 formation, where for each reaction type all combinations of site
638 types are taken into account. The formed CO_2 is assumed to desorb instantaneously and irreversibly due to
639 its weak binding to the surface.

640   In Fig. 9(a) we show the temporal evolution of the system beginning from an initial state corresponding
641 to an empty (20×20) lattice and at 1 bar O_2 and CO pressure and a temperature of 450 K. At these high
642 pressures, it is clear that a substantial fraction of the surface will be covered with O or CO in the final steady
643 state. Indeed, in the very first KMC steps (*i.e.* on nanosecond timescales!), this coverage builds up quickly.
644 The O coverage builds up roughly double as fast as the CO coverage, since every O_2 adsorption event
645 leads to the appearance of two O atoms on the surface in contrast to only one CO in a CO adsorption event.
646 Already after about 20-30 ns one could be mistaken to assume that the system has reached the steady-state
647 solution, since both the TOF and the surface coverages become constant. These coverages roughly reflect
648 the impingement situation, with about 2/3 of all cus and br sites covered by O and about 1/3 of all cus and
649 br sites covered by CO. However, this is not the true steady state! During prolonged KMC simulation (now
650 on a timescale of seconds!) the coverages change again dramatically, until only about 1/3 of all br sites are
651 covered by O (the rest by CO) and essentially all cus sites are covered by CO. In the course of these longer
652 term changes, the TOF decreases by more than three orders of magnitude as compared to the premature
653 apparent steady state. The reason for this two-timescale behavior is that the double as high impingement
654 of O atoms onto the initially empty lattice fills a lot of br sites with oxygen. These O^{br} atoms are very
655 strongly bound and quite unreactive. They will definitely not desorb readily and it requires CO oxidation
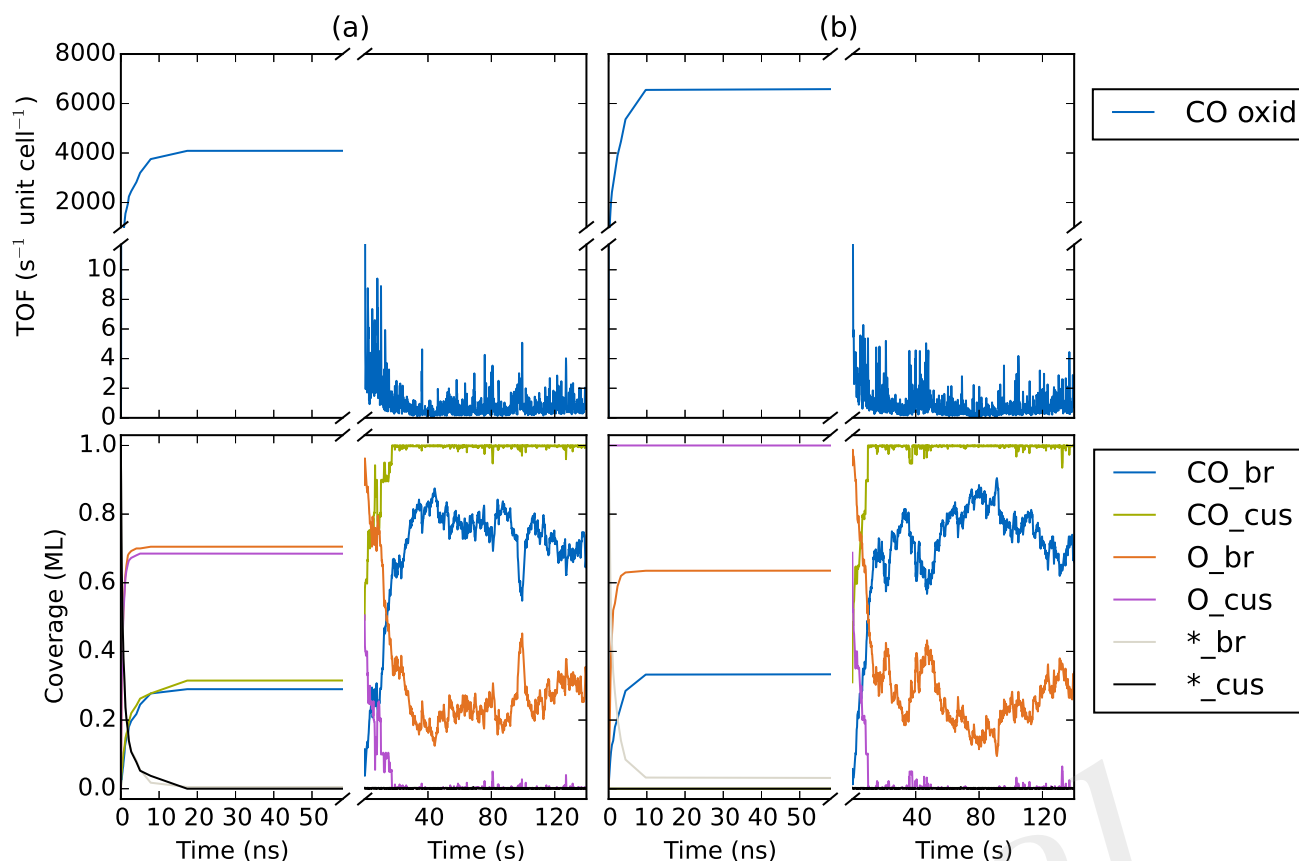
Figure 9. Temporal evolution of (top panel) CO oxidation TOF and (bottom panel) surface coverage of CO, O and vacancies on the cus and bridge sites of the $RuO_2(110)$ lattice. The system is prepared in an initial state corresponding to (a) an empty lattice and (b) 1 ML oxygen coverage on cus sites and vacant bridge sites. The temperature is 450 K and the gas phase CO and O_2 pressures are both 1 bar.

reactions with comparably high barriers (small rate constants) to remove these O^{br} atoms once they have formed. The latter processes therefore take much longer than the initial filling, and since in this longer-term transformation CO also replaces almost all of the highly reactive O^{cus} species, the TOF also collapses.

As impressively demonstrated by this example, identifying what is the true steady state in a KMC simulation can be a major challenge. In fact, this holds even more since what one would really want is to have some form of automatized algorithm that would flag once a simulation has reached steady state. In practical applications, dozens, if not hundreds of different KMC simulations need to be conducted, for instance evaluating different gas phase conditions or determining the influence of changes in the catalyst surface composition (doping with certain metal atoms etc.). It becomes increasingly impractical and cumbersome to having to monitor central quantities of interest during an ongoing KMC simulation and then judge manually whether steady state has been reached. Unfortunately, fully automatic and fool-proof such steady-state detection (SSD) is not yet available for KMC simulations. In contrast, quite some knowledge is for instance available in the area of signal processing and process control Cao and Rhinehart (1995); Kelly and Hedengren (2013). Only very recently such algorithms have also found their way into the KMC community Núñez et al. (2017); Nellis et al. (2018). Typically, they are applied to several properties of interest (reaction rates, coverages, total lattice energy etc.) in order to avoid a false-positive detection of the steady state. Even so, further testing and method development will probably be needed to ascertain whether they can always be applied in a foolproof manner.

674   In the absence of such sophisticated SSD algorithms, one pragmatic approach is often to have a lot of
675 knowledge of the studied system and be really really cautious (certainly not a foolproof and elegant solution
676 though). The other, complementary approach is to start simulations from mindfully chosen varying initial
677 conditions and then monitor if the same steady state is reached. This implies that the system does not
678 exhibit true multiple steady states. Such behavior is well known from the solution of differential equations,
679 for instance in the context of MFA microkinetic models Ramachandran et al. (1981). For KMC simulations
680 in the context of surface catalysis such true multiple steady states that are not the result of a prematurely
681 assumed convergence of the simulation have not been reported, and differentiating between the two cases
682 would likely also be involved. In any case, it never hurts to run several KMC simulations starting from
683 different initial conditions and then monitor where they converge to. Obviously, the closer the initialization
684 is chosen to the final steady state, the faster the simulation will likely converge.

685   Notwithstanding, one might also be trapped in preconceived configurations, when for instance initializing
686 a simulation with a steady-state configuration determined in a preceding (similar) simulation. For the CO
687 oxidation model we illustrate in Fig. 9(b) how starting from a completely different initial population does
688 in fact lead to the same steady state. Here, the initial state corresponded to 1 ML oxygen coverage on the
689 cus sites and vacant bridge sites. For nanosecond timescales we see again the appearance of a (different!)
690 quasi-steady-state solution where the cus sites remain occupied by O, while the bridge sites are covered by
691 about 0.35 ML CO and about 0.65 ML O. However, similar as for the other initialization, on the timescale
692 of seconds the system then transforms again and we arrive at the same steady-state solution as found there.
693 Having understood the reason for this two-timescale behavior, a most suitable initialization would instead
694 be to prepare all br sites with CO to prevent the initial massive buildup of O^{br}. In this case, the true steady
695 state is in fact reached extremely quickly (not shown). Yet, such detailed insight into the chemistry of the
696 system is rarely present in the first place and the approach of starting from largely different initializations
697 is often the best and hopefully reliable shot we have.

698   Once the steady-state solution has been reached, one can make use of the (hopefully present) ergodicity
699 of the KMC simulation to calculate the desired quantities (surface composition, occurrence of various
700 elementary steps, TOFs) as time averages instead of ensemble (trajectory) averages. The average reaction
701 rate, $\langle r^{\beta} \rangle$, for the production of a given molecule β can for instance be calculated as

$$\langle r^{\beta} \rangle = \frac{1}{t_{\mathrm{KMC}}} \sum_{n=1}^{N_{\mathrm{KMC}}} \sum_{j} k_{ij}^{\beta} \Delta t_{\mathrm{escape},n} \quad , \tag{20}$$

702 where t_{KMC} is the total KMC simulation time, the first sum runs over all KMC steps n (up to a total of
703 N_{KMC} steps), the second sum runs over all states j that are accessible from the current state i, k_{ij}^{β} is the
704 rate constant for a process involving the production of the molecule β, and $\Delta t_{\mathrm{escape},n}$ is the escape time
705 for KMC step n. The total simulation time should be chosen long enough to reduce the statistical error
706 on the sampled quantities to a desired value. When calculating statistical errors over successive trajectory
707 fractions, the fraction simulation time must also be chosen long enough that each trajectory fraction is
708 statistically independent of the other fractions. The required time is known as the decorrelation time and it
709 describes the time it takes before the current system configuration is uncorrelated from the initial system
710 configuration in the trajectory fraction. In case the quantity of interest is the transient behavior of the system
711 prepared in a given initial state (*e.g.* to simulate the aforementioned temperature programmed reaction
712 Jansen (1995); Rieger et al. (2008), cyclic voltammetry Rai et al. (2006) or titration Piccinin and Stamatakis
713 (2014) experiments), several statistically independent trajectories must be calculated and averaged. The

714 statistical independence can for example be achieved by using different random number seeds, as was done
715 for the adatom diffusion model in Sec. 5.1 above.

7 SENSITIVITY ANALYSIS AND UNCERTAINTY QUANTIFICATION

716 As already motivated in Sec. 5.1 it can be of particular interest to know the extent to which the rate constants
717 of the various processes in a model influence the model predictions and to thereby quantify the uncertainty
718 of those predictions. This is generally known as sensitivity analysis and uncertainty quantification (UQ).
719 Some of the main questions these methodologies seek to answer are the following: i) Error propagation:
720 How do errors introduced at the level of theory used to calculate rate constants propagate to the model
721 predictions? Which rate constants are most important to calculate with a high accuracy (maybe then
722 recursively refine such calculations once the critical rate constants are known)? What conclusions can
723 be reliably drawn despite the errors? ii) Design and optimization: What are the limitations to achieve an
724 optimal performance of *e.g.* a given catalyst or battery material? How should rate constants be varied (*e.g.*
725 by varying the material) to achieve such optimal performance?

726 One sensitivity measure introduced specifically for catalysis is Campbell's degree of rate control (DRC)
727 $X_{\mathrm{RC},I}$ for reaction step I Campbell (1994)

$$X_{\mathrm{RC},I} = \frac{k_I}{\langle r^\beta \rangle} \left(\frac{\partial \langle r^\beta \rangle}{\partial k_I} \right)_{k_{J \neq I}, K_I} \quad , \tag{21}$$

728 where the average reaction rate $\langle r^\beta \rangle$ should be calculated for the product β of interest and the derivative is
729 evaluated holding constant the rate constants k_J of all other reactions steps J and the equilibrium constant
730 K_I for step I. A positive (negative) DRC signifies that the reaction rate will increase (decrease) when
731 increasing k_I, whereas a value of zero signifies that the reaction rate is insensitive to variations in k_I. The
732 DRCs follow a sum rule, which states that the sum of all DRCs is equal to one Meskine et al. (2009);
733 Hoffmann et al. (2017). A single non-zero DRC equal to one then signifies a single rate-limiting step in the
734 reaction mechanism, while in general several steps can be rate-limiting at the same time. The fact that the
735 equilibrium constant for step I is held constant means that both the forward and reverse rate constants for
736 step I are varied simultaneously, which can also be viewed as a variation of the TS energy of step I (for
737 activated processes). Later, the DRC concept was extended to a thermodynamical version where instead
738 the energies of reaction intermediates are varied Stegelmann et al. (2009). Obviously, these sensitivity
739 measures can easily be extended to other quantities of interest than reaction rates. From a practical point of
740 view, the main challenge in evaluating the derivative entering the DRC expression is that we don't have an
741 analytical expression for the reaction rate in KMC. Relying instead on a finite-difference sampling, very
742 long simulation times are typically required to reduce the statistical error sufficiently Meskine et al. (2009).
743 A more efficient three-stage approach has recently been proposed Hoffmann et al. (2017), which allows for
744 the direct sampling of sensitivity measures from a single KMC trajectory.

745 DRC sensitivity measures are formulated as a linear response theory, meaning that the result is only
746 valid locally in the input parameter space. However, kinetic models are most often highly non-linear
747 and the DRC can change substantially over rate constant variations corresponding to a DFT error of *e.g.*
748 ± 0.2 eV on reaction barriers. Recently, a number of methods have therefore been developed for global
749 sensitivity analysis and UQ, *i.e.* to assess which conclusions about the model can be reliably drawn despite
750 uncertainties in the input parameters Sutton et al. (2016); Döpking and Matera (2017). Ref. Sutton et al.
751 (2016) furthermore addressed the fact that the errors in the input parameters for KMC models are often
752 highly correlated. Such correlations can arise because the used DFT functional might generally over- or

753   underestimate certain kinetic parameters. Corresponding DFT functional correlations have been exploited
754   to assess the uncertainty of reaction rates in a MFA microkinetic model for ammonia synthesis Medford
755   et al. (2014) carried out using the Bayesian error estimation functional with van der Waals correlation
756   (BEEF-vdW) Wellendorff et al. (2012). The latter functional provides not only a single value for a given
757   kinetic parameter, but an ensemble of values generated by sampling known uncertainties in the exchange-
758   correlation model parameters. Another source of correlations in kinetic parameters is the existence of
759   correlations in the adsorption energies of chemically related intermediates and TSs, generally known as
760   scaling relations Nørskov et al. (2002); Michaelides et al. (2003); Abild-Pedersen et al. (2007) (see Sec.
761   4.2.3). Both sources of correlation were considered in the sensitivity analysis and UQ carried out in Ref.
762   Sutton et al. (2016) and applied to a kinetic model for ethanol steam reforming. The method allows to
763   assess whether a proposed reaction mechanism can be considered to agree with experimental data within
764   the known DFT errors and can reveal limitations such as the failure to take into account support effects in
765   heterogeneous catalysis models.

766   To be quite honest, no such sophisticated sensitivity analysis is yet really on the agenda of the large
767   majority of practitioners. As a very crude and simple advise in the context of this practical guide to surface
768   Monte Carlo simulations, we would thus recommend to always at least vary some of the key rate constants
769   in a KMC model by hand and see how this changes the simulation result. This is straightforward to do and it
770   provides a crude (possibly incomplete, but still better than none) picture of what could be the critical input
771   and what are the dependencies in the studied reaction network. In case this flags a critical sensitivity, one
772   can and should escalate from there. Honestly, if the gist of the story one extracts from KMC simulations
773   depends critically on highly specific numerical values of one or a few rate constants and one knows that
774   there is a large uncertainty in these values, then who wants to stick their neck out?

8   TIMESCALE DISPARITY PROBLEM

775   KMC achieves an enormous speedup over MD simulations by avoiding the explicit treatment of the
776   vibrational degrees of freedom of the system, and instead considering only the rare events such as
777   adsorption/desorption, diffusion or reaction steps (see Sec. 2.1). However, also those rare events that are
778   treated in the KMC simulation can occur at largely different timescales. When this is the case, almost all of
779   the CPU time is spent simulating the fast processes, while the (maybe truly important) dynamics arising
780   from the slow processes is sampled insufficiently or not at all. This is especially problematic for KMC
781   models of surface reactions on metals, where often very fast surface diffusion processes and slow surface
782   reactions occur simultaneously in the reaction network.

783   A wide variety of methods has been developed to deal with this timescale disparity problem. The τ-leap
784   method is an approximate procedure in which the KMC simulation is accelerated by the firing of multiple
785   processes at once Gillespie (2001). The underlying assumption (leap condition) of this method is, however,
786   only fulfilled when surface populations are approximately constant during the coarse time increment τ.
787   Hence, the method does not apply to surface reactions on microscopic lattices, where site populations can
788   change dramatically (*e.g.* from zero species to one species) from one KMC step to the next. In practice,
789   the method is only applied to coarse-grained lattices where the concentration of species within one larger
790   coarse-grained cell is approximately constant in time. Other methods rely on a separation of the processes
791   into "slow" and "fast" processes. They treat then only the slow process dynamics stochastically at the KMC
792   level, while the fast process dynamics is treated deterministically or using a Langevin equation Haseltine
793   and Rawlings (2002); Salis and Kaznessis (2005). A main drawback of this class of methods is that the
794   process timescale separation has to be specified by the user in advance and remains fixed throughout the
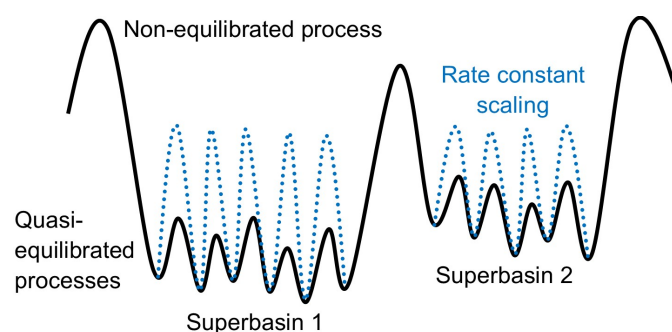795   simulation.

Figure 10. Potential energy surface (PES) for a system with processes occurring at disparate timescales due to large differences in the barriers. A set of states connected by fast (low-barrier), quasi-equilibrated processes constitutes a superbasin. The system can escape from one superbasin to another through the execution of a slow (high barrier), non-equilibrated process. The KMC simulation is accelerated by scaling the rate constants (increasing the barriers) of fast, quasi-equilibrated processes. This decreases the time it takes for the system to leave the current superbasin and thereby enhances the sampling of neighboring regions of the PES (other superbasins).

796   In practice, recent KMC works have therefore often relied on simple acceleration schemes that function
797 by decreasing the rate constants of the fastest processes in the system in order to make the span in process
798 timescales tractable, see Fig. 10. For simple reaction networks such rate constant scaling, together with
799 verification that the model output is not affected by the scaling, can be carried out manually Rogal et al.
800 (2008); Piccinin and Stamatakis (2014); Lorenzi et al. (2016); Jørgensen and Grönbeck (2017). Recently,
801 algorithms have also appeared that take care of the scaling of fast processes automatically, without the
802 user having to specify those processes in advance Chatterjee and Voter (2010); Dybeck et al. (2017). A
803 main assumption of these methods is that fast processes become quasi-equilibrated after a limited number
804 of executions, *i.e.* it is assumed that continued simulation of these processes is not necessary to correctly
805 describe the system dynamics. The accelerated superbasin KMC (AS-KMC) method from Ref. Chatterjee
806 and Voter (2010) defines a superbasin as a set of lattice configurations that the system can jump between
807 through the execution of quasi-equilibrated processes only, see Fig. 10. The execution of a non-equilibrated
808 process then defines the entering of a new superbasin. The goal of the acceleration algorithm thereby
809 becomes to encourage the system to leave the current superbasin at an earlier time through the scaling of
810 fast, quasi-equilibrated processes. A drawback of this method for complex systems is that the total number
811 of system configurations can be very large, which may cause the algorithm to become inefficient since the
812 full sampling of even a single superbasin becomes exceedingly slow.

813   This problem was addressed in the method presented in Ref. Dybeck et al. (2017), where rather than
814 tracking both system configurations (superbasin states) and processes, only the executions of some user-
815 defined reaction channels are tracked. A reaction channel could for example be the adsorption/desorption of
816 some species at a given site type, independently of where on the lattice this reaction occurs, and the scaling
817 of rate constants is then applied to the whole reaction channel. Scaling still only occurs for processes that
818 have been executed a minimum number of times within the current superbasin and for which the number
819 of forward executions is roughly equal to the number of reverse executions to within some tolerance.
820 Once a non-equilibrated process was executed, the rate constants are unscaled again to allow for sufficient
821 sampling of the new superbasin – and the process is started over again. The algorithm was shown to work
822 well for a reaction model of Fischer-Tropsch synthesis over ruthenium nanoparticles Dybeck et al. (2017).
823 Very similar approaches to KMC acceleration, but excluding the unscaling step, have been followed in Refs.
824 Núñez et al. (2017); Hoffmann and Bligaard (2018). In Ref. Núñez et al. (2017) the acceleration scheme

was employed together with efficient sensitivity analysis beyond finite differences (similar to the method from Ref. Hoffmann et al. (2017) that was discussed in the preceding section) for improved sampling of sensitivity measures also in KMC models characterized by large disparities in the timescales.

In Ref. Andersen et al. (2017) the algorithm from Ref. Dybeck et al. (2017) was implemented in the `kmos` code and applied to a trend study of CO methanation over stepped surfaces of the transition metal series using scaling-relation-based rate constant expressions. Also for this more complex reaction mechanism and the consideration of many different catalyst surfaces, the acceleration algorithm generally performed well. However, some challenging cases leading to a breakdown of the algorithm were also identified. A particularly problematic case for the algorithm was shown to be the occurrence of reactions between two low-coverage species, which are both produced in independent, quasi-equilibrated reaction steps. In this case the algorithm may scale the rate constants of the quasi-equilibrated steps too aggressively, leading to insufficient or no sampling of lattice configurations where the two low-coverage species are found at neighboring lattice sites, as required for their reaction. This problem is likely related to the fact that the algorithm from Ref. Dybeck et al. (2017) does not track system configurations and therefore cannot verify if all configurations within a superbasin have been sufficiently sampled. A simple correction scheme that takes into account lattice configurations of the nearest neighbor sites in the definition of the reaction channel was proposed in Ref. Andersen et al. (2017). This was shown to work well for the simple case of a reaction between two low-coverage species formed directly at neighboring sites. However, it does not apply if the low-coverage species are produced at distant lattice sites and rely on diffusion steps before the reaction step.

In some sense it is ironic that KMC is so particularly challenged by fast diffusion steps, considering that its effective competitor in form of MFA microkinetic models is challenged by slow diffusion steps. Even in the absence of lateral interactions, which would generally be used to argue in favor of the validity of the MFA, such slow diffusion processes can prevent the system to ever reach the well-mixed state assumed in the MFA. At metals, this was shown to happen at strongly binding step sites Andersen et al. (2017), whereas at oxides this might arise simply from the higher diffusion barriers at these more open compound materials. For the KMC model of CO oxidation on $RuO_2(110)$ discussed in Sec. 6.1 a corresponding MFA breakdown could for instance be traced back to a relatively high barrier of approximately 1.6 eV for O diffusion Temel et al. (2007); Matera et al. (2011); Exner et al. (2015). In this respect, this leaves essentially no system of interest in surface catalysis where one could generally expect mean-field kinetics to yield the right answers: At metals, the MFA is typically invalidated by strong lateral interactions at nearby sites (see next section), at compounds like oxides high diffusion barriers prevent a sufficient mixing of the adsorption layer. The problem is then that even though modern KMC implementations like those discussed in Sec. 3 have become dramatically more efficient, they are typically still more demanding than mean-field models. The timescale disparity problem adds significantly to this and even though most recent acceleration algorithms have become better, this problem is not yet fully solved. This still leaves many users to resort to MFA microkinetic modeling, even though it is likely not correct. Alternatively, algorithms that are intermediate between MFA and KMC in terms of accuracy and computational cost such as the quasichemical approximation have also been applied to catalytic reactions Hellman and Honkala (2007) and have in some cases been shown to reproduce KMC simulations at significantly reduced cost.

9 LATERAL INTERACTIONS

Lateral interactions are interactions between species adsorbed to a lattice. They can be either attractive or repulsive depending on the chemical nature of the involved species and the surface or bulk material defining the KMC lattice. Several recent studies have found that lateral interactions are essential to take

868 into account for a correct description of the system dynamics Stamatakis and Piccinin (2016); Jørgensen
869 and Grönbeck (2017); Piccinin and Stamatakis (2017); Vignola et al. (2017); Hus and Hellman (2019). As
870 already discussed in Sec. 2.2, lateral interactions are taken into account within the lattice approximation
871 in KMC by assigning an individual hopping rate constant to each neighbor configuration (see Fig. 3). In
872 case of repulsive interactions, the particle will be more likely to jump away from an initial configuration
873 with occupied neighboring sites as compared to empty neighboring sites. This will cause the particles to
874 spread out over the lattice to maximize the inter-particle distances. For attractive interactions, the situation
875 is exactly opposite and the particles will show a tendency for island formation. Both cases can lead to
876 the formation of ordered structures on the lattice. They may therefore lead to inaccuracies of mean-field
877 treatments of the system kinetics, since the MFA assumes a random distribution of the particles without any
878 correlations between sites Liu et al. (2016); Stamatakis and Piccinin (2016); Pineda and Stamatakis (2017).

879   In practice, lateral interactions can be accounted for in lattice KMC models through the general cluster
880 expansion method Sanchez et al. (1984); Stampfl et al. (1999); Müller (2003). In this method, the lattice
881 energy is expanded into a sum of discrete interactions (clusters) such as pairwise interactions, three-body
882 interactions etc. through a lattice-gas Hamiltonian. For any adsorbate on the lattice, one would thus
883 evaluate how many neighbors of which type sit at which kind of distances (nearest-neighbor, next nearest
884 neighbor etc.). For each such neighbor the adsorption energy (or more generally rate constant) of an
885 isolated particle on the lattice at this site type would be corrected for by a certain amount prescribed
886 by the lattice-gas Hamiltonian. Summing up all these contributions defines the pairwise interactions.
887 Then one looks up all possible motifs of two simultaneously present neighboring species, for which
888 again there are energy (rate constant) corrections. This defines the three-body corrections to the pairwise
889 interaction correction, and formally this goes on to higher and higher many-body interactions. While cluster
890 expansions considering up to three- and four-body terms have been parametrized with DFT for simple
891 systems Jansen and Offermans (2005); Zhang et al. (2007); Schmidt et al. (2012); Wu et al. (2012); Piccinin
892 and Stamatakis (2014), presently cluster expansions are typically truncated already after the first nearest
893 neighbor pairwise interaction term in more complex systems with many species and site types in order to
894 keep the computational cost tractable Stamatakis and Vlachos (2011); Yang et al. (2013). A particularly
895 crude form of this are so-called site-blocking rules Hoffmann and Reuter (2014); Lorenzi et al. (2016); Liu
896 et al. (2016), where strongly repulsive first neighbor interactions are simply modeled by suppressing any
897 KMC processes that would lead to such immediately neighboring species. Furthermore, cluster expansions
898 are typically used only for adsorbates in their stable and metastable adsorption sites, since taking into
899 account also transition states, *i.e.* changes in barrier heights due to lateral interactions, could make the DFT
900 parametrization intractable. In the ZACROS KMC code cluster expansion is built-in for adsorbates and
901 the effect of lateral interactions on transition states is instead taken into account through an approximate
902 Brønsted-Evans-Polanyi relation Nielsen et al. (2013). A main drawback of the cluster expansion method
903 is that the computational cost of both the DFT parametrization and the KMC simulation can quickly
904 become intractable for complex systems. A benchmarking of the cluster expansion parametrized in Ref.
905 Wu et al. (2012) showed that the computational cost of the KMC simulation increased with about 5 orders
906 of magnitude when the number of clusters considered increased from 3 to 12 Nielsen et al. (2013). Of
907 course, this depends on the actual KMC implementation and algorithm used, and in particular codes like
908 ZACROS are written to mitigate the additional costs when considering lateral interactions.

909   Despite the added cost, we emphasize again that lateral interactions often play an important role not only
910 for surface diffusion, but also for crystal growth and heterogeneous catalysis. In the following we will thus
911 provide two example kmos models for the application areas crystal growth and heterogeneous catalysis
912 that take into account lateral interactions. For more realistic growth and lateral interaction models we refer

913 to the literature Fichthorn et al. (2002); Ruan and Schuh (2010); Shirazi and Elliott (2014).

914
915 ## 9.1 `kmos` **models with lateral interactions**

916 We will begin this section with a short description of two of the available `kmos` backends and the way
917 they each handle lateral interactions. The *local smart* backend is the original backend and has been used
918 as a basis and inspiration for the other backends. It was built with the implicit objective of offering the
919 best run time possible at the expense of memory usage. For this reason, a key element in this backend is
920 a pre-calculated list of rate constants, *i.e.* a *rate catalog*. Together with an efficient local updating of the
921 available processes after each KMC step, this makes it the most efficient backend when the number of
922 different rate constants in the list is reasonable small. The *local smart* backend implements the most simple
923 treatment of lateral interactions, in which any new neighbor configuration defines a new KMC process with
924 a rate constant associated with this particular configuration. There are several drawbacks of this approach
925 for models with lateral interactions since these generally feature an exponentially growing number of
926 processes with the number of interactions taken into account: (i) Several routines whose execution time
927 scale with the total number of processes can become slow, (ii) the bookkeeping data structures, which scale
928 in size with the total number of processes, can become too big for available memory, (iii) the size of the
929 source code can become very large, making compilation very slow or even impossible due to memory
930 requirements.

931 The *on-the-fly* backend was constructed to alleviate the problems encountered in the *local smart* backend
932 and to enable KMC simulations of complex lateral interaction models. As the name implies, it calculates
933 rate constants *on-the-fly* instead of making use of a pre-calculated rate catalog. In the *on-the-fly* backend
934 the local environment is taken into account for each process through a *bystander* list. Here a bystander is a
935 neighboring site whose occupation influences the rate constant of the process according to the on-the-fly-
936 calculated rate constant. The benefit of this approach is that the total number of processes in the model is
937 constant with respect to the number of interactions taken into account. On the other hand, the drawback is
938 that now the compute time of each KMC step scales linearly with the system size due to the need to scan
939 through the lattice and sum up all rate constants explicitly in order to evaluate the total escape rate constant
940 k_{tot} (Eq. 9).

941 Now moving to examples, we will first present a `kmos` model for crystal growth with lateral interactions
942 that is simple enough that it can be handled efficiently in the *local smart* backend. For this model we
943 consider a three-dimensional quadratic lattice and a single species that is deposited onto a solid substrate
944 with a constant adsorption rate constant $k_{\mathrm{ads}} = 3 \cdot 10^{-3} \, \mathrm{s}^{-1}$. The low-coverage desorption barrier ΔE_0 is
945 set to 1 eV. In addition, we consider attractive pairwise lateral interactions $\epsilon_{\mathrm{int}} = 0.5 \, \mathrm{eV}$ with the nearest
946 neighbor species. Thereby, the rate constant for the desorption process k_{des} becomes

$$k_{\mathrm{des}} = \frac{k_{\mathrm{B}}T}{h} \exp\left(-\frac{\Delta E_0 + n_{\mathrm{NN}} \cdot \epsilon_{\mathrm{int}}}{k_{\mathrm{B}}T}\right) \quad , \tag{22}$$

947 where n_{NN} is the number of nearest neighbor species in the lattice configuration. For the desorption process
948 to be possible the species must be located in the surface layer, *i.e.* the site just below it must be occupied
949 and the site just above it must be empty. Lateral interactions are then taken into account for the four
950 neighboring sites at the same z height, see Fig. 11(a). Since there are only two possible configurations for
951 each neighbor site (empty or occupied) this leads to merely 16 inequivalent desorption process types and
952 this model can therefore be efficiently treated in the *local smart* backend.
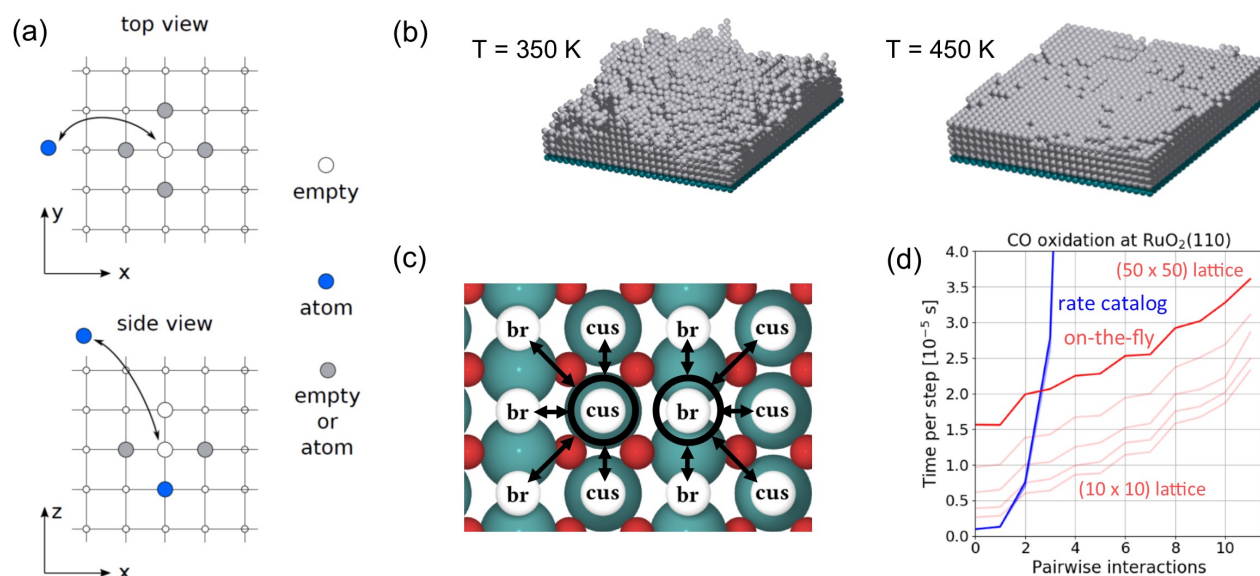
Figure 11. (a) Illustration of the lateral interaction model for the desorption process of the crystal growth model. The site just below the desorbing species is always occupied and its interaction energy is therefore included in the low-coverage desorption barrier. The four neighboring sites at the same z height can be either empty or occupied and modify the desorption rate constant accordingly. (b) Snapshots of grown crystal structures at two different temperatures. (c) Illustration of pairwise interactions in the CO oxidation on $RuO_2(110)$ model. (d) kmos performance for the CO oxidation model as a function of the number of pairwise interactions considered for two different backends (rate catalog or on-the-fly calculation of rate constants). Using a rate catalog, the performance is independent of the lattice size. In the on-the-fly implementation the cost instead grows linearly with the lattice size (quadratic growth with the length N of an $(N \times N)$ simulation cell) as illustrated for N equal to 10, 20, 30, 40, 50 (different red lines).

953   In Fig. 11(b) we show snapshots of the grown crystal structure for temperatures of 350 K and 450 K. In
954 both simulations the system is prepared in an initial state corresponding to one layer of fixed substrate
955 species (blue atoms) onto which adsorption can take place. As expected, the grown structure becomes
956 smoother at higher temperatures, where atoms deposited onto unfavorable adsorption sites with no attractive
957 interactions to neighboring species will be more likely to desorb. The model could be made more realistic
958 by including also diffusion processes and by considering a more detailed cluster expansion model for the
959 lateral interactions.

960   As the next example we return to the catalysis model for CO oxidation on $RuO_2(110)$ already discussed
961 in Sec. 6.1. To explore how the kmos performance of the *local smart* and *on-the-fly* backends are each
962 affected by increasingly complex lateral interaction models, we step-wise add pairwise interactions to each
963 process in the model. Possible pairwise interactions are illustrated with black arrows in Fig. 11(c) for a
964 second-order process (*e.g.* O_2 desorption) involving two neighboring sites (marked with black circles). The
965 performance of each backend as a function of the number of interactions included is shown in Fig. 11(d).
966 For the *local smart* backend (rate catalog) the cost grows exponentially with the number of interactions
967 and we are effectively limited to simple interaction models with a maximum of four pair-wise interactions.
968 This happens because the number of processes in the rate catalog grows exponentially with the number of
969 interactions, *i.e.* the three possible occupations of each neighboring site (O, CO or empty) to the power of
970 the number of neighboring sites (interactions) taken into account. In the *on-the-fly* backend the cost grows
971 only linear with the number of interactions and remains tractable at all considered system sizes, despite
972 the quadratic scaling of the cost with the length N of the $(N \times N)$ simulation cell used (linear scaling

973 with system size). It is worth noting in this context that the *on-the-fly* algorithm presented here specifically
974 for `kmos` is not new. For example, also the ZACROS code Nielsen et al. (2013) calculates rate constants
975 *on-the-fly*.

976 As has hopefully become evident from the above examples, lateral interactions are a double-edged sword
977 for KMC models. On the one hand, the ability to systematically take into account effects of the local
978 environment through systematic cluster expansion enables models of potentially very high accuracy and
979 constitutes a great advantage over MFA models. On the other hand, the inclusion of lateral interactions
980 counteracts the reduction in the number of needed first-principles rate constants that was obtained by
981 making use of the lattice approximation (see Sec. 2.2) and introduces additional complexity and cost to
982 the KMC simulation. In practice, the choice of lateral interaction model therefore (unfortunately) often
983 becomes a pragmatic one determined by what is computationally feasible, even if it is well-known that an
984 appropriate interaction model can be crucial for the validity of the kinetic model.

10   SUMMARY AND OUTLOOK

985 The last decade has witnessed an impressive growth, not only in the number of studies employing predictive,
986 first-principles KMC modeling, but also in the number of new codes that have become available. Especially
987 for heterogeneous catalysis applications, the employed models are increasingly able to deal with complexity,
988 both in the employed reaction mechanisms and in the structure of the catalytic material modeled. These
989 advances have been powered by algorithmic developments for the determination of the input processes and
990 rate constants, as well as for the actual algorithms that carry out the KMC simulation.

991 With many new KMC users entering this exciting field, the aim of this tutorial review has been to provide
992 the necessary practical guidelines and examples for constructing and evaluating KMC models, and to
993 highlight the pitfalls met along the way as well as current challenges and perspectives. We discussed
994 in detail how to make use of the *lattice approximation* in order to exploit a crystalline symmetry of the
995 underlying surface lattice and thereby reduce the number of required first-principles rate constants. This
996 also involves pitfalls and challenges, in particular when a dynamical restructuring of the surface takes
997 place, or if well-defined adsorption sites of the surface species do not exist. We briefly discussed how
998 *off-lattice* (adaptive) KMC attempts to overcome these limitations, as well as the limitations associated
999 with a pre-defined – possibly incomplete – list of possible processes, through the automatic identification of
1000 possible states and processes. However, despite this exciting perspective, these methods are still hampered
1001 by their high cost in practice.

1002 Even for *lattice* KMC models the number of required first-principles rate constants can be daunting.
1003 Prevalent TST approaches require the location of the TS and often also the determination of prefactors and
1004 zero-point vibrational energies, at least to the level of determining the harmonic frequencies of the system.
1005 While it is desirable to carry out these calculations by DFT or other electronic structure methods to achieve
1006 a predictive-quality model, the development of cheaper methods could dramatically increase the complexity
1007 that it is possible to tackle. To this end, we discussed commonly employed BEP and scaling relations as one
1008 prevalent example today. For the future, the development of increasingly accurate semi-empirical methods
1009 such as Density-Functional Tight-Binding (DFTB), reactive force fields or machine-learning-based force
1010 fields is an interesting perspective to which we ascribe a high potential. The actual determination of the
1011 TS is typically the computational bottleneck, and for this we discussed a number of methods and their
1012 respective strong and weak points. Furthermore, we discussed how the accuracy of the employed rate
1013 constants can be systematically improved in *lattice* KMC models through the cluster expansion method in
1014 cases where the local environment significantly influences the rate constant.

1015 For KMC models constructed using first-principles DFT rate constants, one still has to bear in mind
1016 that the expected error on barriers can easily be on the order of several hundreds of meV. This may
1017 lead to rate constants that are potentially wrong by orders of magnitude. A practical way to tackle this
1018 significant drawback is to estimate the sensitivity of the model predictions on the input rate constants and
1019 to quantify the uncertainties on those predictions. For this, we discussed various approaches ranging from a
1020 simple parameter variation to sophisticated models taking into account correlations between the input rate
1021 constants. An exciting perspective here is a recurrent refinement of the used rate constants, possibly also
1022 regarding the lateral interaction model employed, as information about the importance of the various input
1023 processes becomes increasingly available.

1024 While KMC has come a long way, there are also a number of challenges to be met in the future. One
1025 example of this is the inevitable timescale disparity problem, which continues to challenge practical
1026 applications of KMC. We discussed a wide variety of methods that have appeared in the last decades, with
1027 a particular focus on recent acceleration algorithms that automatically identify the simulation bottlenecks,
1028 *i.e.* the fast, quasi-equilibrated processes. While these approaches can work well in many cases, there are
1029 also examples where they break down. Likely, this is an area where further improvements are to be seen in
1030 the coming years.

CONFLICT OF INTEREST STATEMENT

1031 The authors declare that the research was conducted in the absence of any commercial or financial
1032 relationships that could be construed as a potential conflict of interest.

AUTHOR CONTRIBUTIONS

1033 The manuscript was written jointly by all co-authors.

FUNDING

ACKNOWLEDGMENTS

SUPPLEMENTAL DATA

1040 All files required to set up and run the KMC models described in the text with the `kmos` code as well as a
1041 text document with additional explanations are provided as supplemental data.

REFERENCES

1042 Abild-Pedersen, F., Greeley, J., Studt, F., Rossmeisl, J., Munter, T. R., Moses, P. G., et al. (2007). Scaling
1043   properties of adsorption energies for hydrogen-containing molecules on transition-metal surfaces. *Phys.*
1044   *Rev. Lett.* 99, 016105
1045 Andersen, M., Plaisance, C. P., and Reuter, K. (2017). Assessment of mean-field microkinetic models for
1046   co methanation on stepped metal surfaces using accelerated kinetic monte carlo. *J. Chem. Phys.* 147,
1047   152705

1048 Bassett, D. and Webber, P. (1978). Diffusion of single adatoms of platinum, iridium and gold on platinum
1049   surfaces. *Surf. Sci.* 70, 520 – 531

1050 Bortz, A., Kalos, M., and Lebowitz, J. (1975). A new algorithm for monte carlo simulation of ising spin
1051   systems. *J. Comput. Phys* 17, 10–18

1052 Campbell, C. T. (1994). Future directions and industrial perspectives micro- and macro-kinetics: Their
1053   relationship in heterogeneous catalysis. *Top. Catal.* 1, 353–366

1054 Cao, S. and Rhinehart, R. (1995). An efficient method for on-line identification of steady state. *J. Process*
1055   *Contr.* 5, 363 – 374

1056 Carilli, M. F., Delaney, K. T., and Fredrickson, G. H. (2015). Truncation-based energy weighting string
1057   method for efficiently resolving small energy barriers. *J. Chem. Phys.* 143, 054105

1058 Chatterjee, A. and Vlachos, D. G. (2007). An overview of spatial microscopic and accelerated kinetic
1059   monte carlo methods. *J. Comput. Aided Mater. Des.* 14, 253–308

1060 Chatterjee, A. and Voter, A. F. (2010). Accurate acceleration of kinetic monte carlo simulations through
1061   the modification of rate constants. *J. Chem. Phys.* 132, 194101

1062 Chill, S. T. and Henkelman, G. (2014). Molecular dynamics saddle search adaptive kinetic monte carlo. *J.*
1063   *Chem. Phys.* 140, 214110

1064 Chorkendorff, I. and Niemantsverdriet, J. W. (2017). *Concepts of Modern Catalysis and Kinetics, 3rd*
1065   *Edition* (Wiley)

1066 Döpking, S. and Matera, S. (2017). Error propagation in first-principles kinetic monte carlo simulation.
1067   *Chem. Phys. Lett.* 674, 28 – 32

1068 Dybeck, E. C., Plaisance, C. P., and Neurock, M. (2017). Generalized temporal acceleration scheme for
1069   kinetic monte carlo simulations of surface catalytic processes by scaling the rates of fast reactions. *J.*
1070   *Chem. Theory Comput.* 13, 1525–1538

1071 Exner, K. S., Heß, F., Over, H., and Seitsonen, A. P. (2015). Combined experiment and theory approach in
1072   surface chemistry: Stairway to heaven? *Surf. Sci.* 640, 165 – 180

1073 Feibelman, P. J. (1990). Diffusion path for an al adatom on al(001). *Phys. Rev. Lett.* 65, 729–732

1074 Fichthorn, K., Merrick, M., and Scheffler, M. (2002). A kinetic monte carlo investigation of island
1075   nucleation and growth in thin-film epitaxy in the presence of substrate-mediated interactions. *Appl. Phys.*
1076   *A* 75, 17–23

1077 Fichthorn, K. A. and Weinberg, W. H. (1991). Theoretical foundations of dynamical monte carlo
1078   simulations. *J. Chem. Phys.* 95, 1090–1096

1079 Frenkel, D. and Smit, B. (2001). *Understanding Molecular Simulation: From Algorithms to Applications*
1080   *(Computational Science Series, Vol 1)* (Academic Press)

1081 Garhammer, A. (2017). *kMC-simulation of magnetic resonance spectra of ion dynamics in all-solid-state*
1082   *Li ion batteries*. Master's thesis, Technical University of Munich, Department of Physics

1083 Gelten, R. J., Jansen, A. P. J., van Santen, R. A., Lukkien, J. J., Segers, J. P. L., and Hilbers, P. A. J. (1998).
1084   Monte carlo simulations of a surface reaction model showing spatio-temporal pattern formations and
1085   oscillations. *J. Chem. Phys.* 108, 5921–5934

1086 Gillespie, D. T. (1976). A general method for numerically simulating the stochastic time evolution of
1087   coupled chemical reactions. *J. Chem. Phys.* 22, 403–434

1088 Gillespie, D. T. (2001). Approximate accelerated stochastic simulation of chemically reacting systems. *J.*
1089   *Chem. Phys.* 115, 1716–1733

1090 Halgren, T. A. and Lipscomb, W. N. (1977). The synchronous-transit method for determining reaction
1091   pathways and locating molecular transition states. *Chem. Phys. Lett.* 49, 225–232

Haseltine, E. L. and Rawlings, J. B. (2002). Approximate simulation of coupled fast and slow reactions for stochastic chemical kinetics. *J. Chem. Phys.* 117, 6959–6969

Hellman, A. and Honkala, K. (2007). Including lateral interactions into microkinetic models of catalytic reactions. *J. Chem. Phys.* 127, 194704

Henkelman, G., Jóhannesson, G., and Jónsson, H. (2002). Methods for finding saddle points and minimum energy paths. In *Theoretical Methods in Condensed Phase Chemistry*, ed. S. D. Schwartz (Dordrecht: Springer Netherlands). 269–302

Henkelman, G. and Jónsson, H. (1999). A dimer method for finding saddle points on high dimensional potential surfaces using only first derivatives. *J. Chem. Phys.* 111, 7010–7022

Henkelman, G. and Jónsson, H. (2000). Improved tangent estimate in the nudged elastic band method for finding minimum energy paths and saddle points. *J. Chem. Phys.* 113, 9978–9985

Henkelman, G. and Jónsson, H. (2001). Long time scale kinetic monte carlo simulations without lattice approximation and predefined event table. *J. Chem. Phys.* 115, 9657–9666

Henkelman, G., Uberuaga, B. P., and Jónsson, H. (2000). A climbing image nudged elastic band method for finding saddle points and minimum energy paths. *J. Chem. Phys.* 113, 9901–9904

Hoffmann, M. J. and Bligaard, T. (2018). A lattice kinetic monte carlo solver for first-principles microkinetic trend studies. *J. Chem. Theory Comput.* 14, 1583–1593

Hoffmann, M. J., Engelmann, F., and Matera, S. (2017). A practical approach to the sensitivity analysis for kinetic monte carlo simulation of heterogeneous catalysis. *J. Chem. Phys.* 146, 044118

Hoffmann, M. J., Matera, S., and Reuter, K. (2014). kmos: A lattice kinetic monte carlo framework. *Comput. Phys. Commun.* 185, 2138 – 2150

Hoffmann, M. J. and Reuter, K. (2014). Co oxidation on pd(100) versus pdo(101)-($sqrt5 \times sqrt5$)$r27\circ$: First-principles kinetic phase diagrams and bistability conditions. *Top. Catal.* 57, 159–170

Hohenberg, P. and Kohn, W. (1964). Inhomogeneous Electron Gas. *Phys. Rev.* 136, B864–B871

Hus, M. and Hellman, A. (2019). Ethylene epoxidation on ag(100), ag(110), and ag(111): A joint ab initio and kinetic monte carlo study and comparison with experiments. *ACS Catal.* 9, 1183–1196

Ionova, I. V. and Carter, E. A. (1993). Ridge method for finding saddle points on potential energy surfaces. *J. Chem. Phys.* 98, 6377–6386

Janardhanan, V. M. and Deutschmann, O. (2011). Computational fluid dynamics of catalytic reactors. In *Modeling and Simulation of Heterogeneous Catalytic Reactions* (Wiley-VCH Verlag GmbH & Co. KGaA). 251–282

Jansen, A. (1995). Monte carlo simulations of chemical reactions on a surface with time-dependent reaction-rate constants. *Comput. Phys. Commun.* 86, 1–12

Jansen, A. P. J. and Offermans, W. K. (2005). Lateral interactions in o/pt(111): Density-functional theory and kinetic monte carlo. In *Computational Science and Its Applications – ICCSA 2005*, eds. O. Gervasi, M. L. Gavrilova, V. Kumar, A. Laganà, H. P. Lee, Y. Mun, D. Taniar, and C. J. K. Tan (Berlin, Heidelberg: Springer), 1020–1029

Jónsson, H., Mills, G., and Jacobsen, K. W. (1998). Nudged elastic band method for finding minimum energy paths of transitions. In *Classical and Quantum Dynamics in Condensed Phase Simulations*, ed. B. J. Berne (World Scientific). 385–404

Jørgensen, M. and Grönbeck, H. (2017). Scaling relations and kinetic monte carlo simulations to bridge the materials gap in heterogeneous catalysis. *ACS Catal.* 7, 5054–5061

Jørgensen, M. and Grönbeck, H. (2018). MonteCoffee: A programmable kinetic monte carlo framework. *J. Chem. Phys.* 149, 114101

1136 Kelly, J. D. and Hedengren, J. D. (2013). A steady-state detection (ssd) algorithm to detect non-stationary
1137   drifts in processes. *J. Process Contr.* 23, 326 – 331

1138 Kohn, W. and Sham, L. J. (1965). Self–Consistent Equations Including Exchange and Correlation Effects.
1139   *Phys. Rev.* 140, A1133–A1138

1140 Kolsbjerg, E. L., Groves, M. N., and Hammer, B. (2016). An automated nudged elastic band method. *J.*
1141   *Chem. Phys.* 145, 094107

1142 Konwar, D., Bhute, V. J., and Chatterjee, A. (2011). An off-lattice, self-learning kinetic monte carlo
1143   method using local environments. *J. Chem. Phys.* 135, 174103

1144 Laidler, K. J. (1987). *Chemical Kinetics* (New York: Harper & Row)

1145 Liu, D.-J., Zahariev, F., Gordon, M. S., and Evans, J. W. (2016). Predictive beyond-mean-field rate
1146   equations for multisite lattice–gas models of catalytic surface reactions: Co oxidation on pd(100). *J.*
1147   *Phys. Chem. C* 120, 28639–28653

1148 Lorenzi, J. M., Matera, S., and Reuter, K. (2016). Synergistic inhibition of oxide formation in oxidation
1149   catalysis: A first-principles kinetic monte carlo study of no + co oxidation at pd(100). *ACS Catal.* 6,
1150   5191–5197

1151 Margraf, J. T. and Reuter, K. (2019). Systematic enumeration of elementary reaction steps in surface
1152   catalysis. *ACS Omega* 4, 3370–3379

1153 Matera, S., Maestri, M., Cuoci, A., and Reuter, K. (2014). Predictive-quality surface reaction chemistry in
1154   real reactor models: Integrating first-principles kinetic monte carlo simulations into computational fluid
1155   dynamics. *ACS Catal.* 4, 4081–4092

1156 Matera, S., Meskine, H., and Reuter, K. (2011). Adlayer inhomogeneity without lateral interactions:
1157   Rationalizing correlation effects in co oxidation at ruo2(110) with first-principles kinetic monte carlo. *J.*
1158   *Chem. Phys.* 134, 064713

1159 Matera, S. and Reuter, K. (2010). Transport limitations and bistability for in situ co oxidation at $ruo_2(110)$:
1160   First-principles based multiscale modeling. *Phys. Rev. B* 82, 085446

1161 Medford, A. J., Shi, C., Hoffmann, M. J., Lausche, A. C., Fitzgibbon, S. R., Bligaard, T., et al. (2015).
1162   Catmap: A software package for descriptor-based microkinetic mapping of catalytic trends. *Catal. Lett.*
1163   145, 794–807

1164 Medford, A. J., Wellendorff, J., Vojvodic, A., Studt, F., Abild-Pedersen, F., , K. W., et al. (2014). Assessing
1165   the reliability of calculated catalytic ammonia synthesis rates. *Science* 345, 197–200

1166 Meskine, H., Matera, S., Scheffler, M., Reuter, K., and Metiu, H. (2009). Examination of the concept of
1167   degree of rate control by first-principles kinetic monte carlo simulations. *Surf. Sci.* 603, 1724 – 1730

1168 Mhadeshwar, A. B., Wang, H., and Vlachos, D. G. (2003). Thermodynamic consistency in microkinetic
1169   development of surface reaction mechanisms. *J. Phys. Chem. B* 107, 12721–12733

1170 Michaelides, A., Liu, Z.-P., Zhang, C. J., Alavi, A., King, D. A., and Hu, P. (2003). Identification of
1171   general linear relationships between activation energies and enthalpy changes for dissociation reactions
1172   at surfaces. *J. Am. Chem. Soc.* 125, 3704–3705

1173 Müller, S. (2003). Bulk and surface ordering phenomena in binary metal alloys. *J. Phys. Condens. Matter*
1174   15, R1429

1175 Nellis, C., Danielson, T., Savara, A., and Hin, C. (2018). The f-t-pj-rg method: An adjacent-rolling-
1176   windows based steady-state detection technique for application to kinetic monte carlo simulations.
1177   *Comput. Phys. Commun.* 232, 124 – 138

1178 Nielsen, J., d'Avezac, M., Hetherington, J., and Stamatakis, M. (2013). Parallel kinetic monte carlo
1179   simulation framework incorporating accurate models of adsorbate lateral interactions. *J. Chem. Phys.*
1180   139, 224706

1181 Nørskov, J. K., Bligaard, T., Logadottir, A., Bahn, S., Hansen, L. B., Bollinger, M., et al. (2002).
1182   Universality in heterogeneous catalysis. *J. Catal.* 209, 275

1183 Núñez, M., Robie, T., and Vlachos, D. G. (2017). Acceleration and sensitivity analysis of lattice kinetic
1184   monte carlo simulations using parallel processing and rate constant rescaling. *J. Chem. Phys.* 147,
1185   164103

1186 Pedersen, A., Karssemeijer, L., Cuppen, H. M., and Jónsson, H. (2015). Long-time-scale simulations of
1187   h2o admolecule diffusion on ice ih(0001) surfaces. *J. Phys. Chem. C* 119, 16528–16536

1188 Peters, B., Heyden, A., Bell, A. T., and Chakraborty, A. (2004). A growing string method for determining
1189   transition states: Comparison to the nudged elastic band and string methods. *J. Chem. Phys.* 120,
1190   7877–7886

1191 Piccinin, S. and Stamatakis, M. (2014). Co oxidation on pd(111): A first-principles-based kinetic monte
1192   carlo study. *ACS Catal.* 4, 2143–2152

1193 Piccinin, S. and Stamatakis, M. (2017). Steady-state co oxidation on pd(111): First-principles kinetic
1194   monte carlo simulations and microkinetic analysis. *Top. Catal.* 60, 141–151

1195 Pineda, M. and Stamatakis, M. (2017). Beyond mean-field approximations for accurate and computationally
1196   efficient models of on-lattice chemical kinetics. *J. Chem. Phys.* 147, 024105

1197 Rai, V., Pitsch, H., and Novikov, A. (2006). Efficient dynamic monte carlo algorithm for time-dependent
1198   catalytic surface chemistry. *Phys. Rev. E* 74, 046707

1199 Raimondeau, S. and Vlachos, D. (2002). Recent developments on multiscale, hierarchical modeling of
1200   chemical reactors. *Chem. Eng. J.* 90, 3–23

1201 Ramachandran, P. A., Kulkarni, B. D., and Sadana, A. (1981). Analysis of multiple steady states of
1202   complex biochemical reactions. *J. Chem. Technol. Biotechnol.* 31, 546–552

1203 Reuter, K. (2011). First-principles kinetic monte carlo simulations for heterogeneous catalysis: Conce-
1204   pts, status, and frontiers. In *Modeling and Simulation of Heterogeneous Catalytic Reactions*, ed.
1205   O. Deutschmann (Weinhein: Wiley). 71–111

1206 Reuter, K. (2016). Ab initio thermodynamics and first-principles microkinetics for surface catalysis. *Catal.*
1207   *Lett.* 146, 541–563

1208 Reuter, K., Frenkel, D., and Scheffler, M. (2004). The steady state of heterogeneous catalysis, studied by
1209   first-principles statistical mechanics. *Phys. Rev. Lett.* 93, 116105

1210 Reuter, K. and Scheffler, M. (2006). First-principles kinetic monte carlo simulations for heterogeneous
1211   catalysis: Application to the co oxidation at $Ruo_2(110)$. *Phys. Rev. B* 73, 045433

1212 Reuter, K., Stampf, C., and Scheffler, M. (2005). Ab initio atomistic thermodynamics and statistical
1213   mechanics of surface properties and functions. In *Handbook of Materials Modeling: Methods*, ed. S. Yip
1214   (Dordrecht: Springer Netherlands). 149–194

1215 Rieger, M., Rogal, J., and Reuter, K. (2008). Effect of surface nanostructure on temperature programmed
1216   reaction spectroscopy: First-principles kinetic monte carlo simulations of co oxidation at $ruo_2(110)$.
1217   *Phys. Rev. Lett.* 100, 016105

1218 Rogal, J., Reuter, K., and Scheffler, M. (2008). Co oxidation on pd(100) at technologically relevant
1219   pressure conditions: First-principles kinetic monte carlo study. *Phys. Rev. B* 77, 155410

1220 Rothman, M. J. and Lohr, L. L. (1980). Analysis of an energy minimization method for locating transition
1221   states on potential energy hypersurfaces. *Chem. Phys. Lett.* 70, 405–409

1222 Ruan, S. and Schuh, C. A. (2010). Kinetic monte carlo simulations of nanocrystalline film deposition. *J.*
1223   *Appl. Phys.* 107, 073512

1224 Sabbe, M., Reyniers, M.-F., and Reuter, K. (2012). First-principles kinetic modeling in heterogeneous
1225   catalysis: an industrial perspective on best-practice, gaps and needs. *Cat. Sci. Technol.* 2, 2010

Salis, H. and Kaznessis, Y. (2005). Accurate hybrid stochastic simulation of a system of coupled chemical or biochemical reactions. *J. Chem. Phys.* 122, 054103

Sanchez, J., Ducastelle, F., and Gratias, D. (1984). Generalized cluster description of multicomponent systems. *Physica A* 128, 334 – 350

Schmidt, D. J., Chen, W., Wolverton, C., and Schneider, W. F. (2012). Performance of cluster expansions of coverage-dependent adsorption of atomic oxygen on pt(111). *J. Chem. Theory Comput.* 8, 264–273

Schmitz, G. (2000). Thermodynamic consistency of reaction mechanisms and null cycles. *J. Chem. Phys.* 112, 10714–10717

Shirazi, M. and Elliott, S. D. (2014). Atomistic kinetic monte carlo study of atomic layer deposition derived from density functional theory. *J. Comput. Chem.* 35, 244–259

Slepoy, A., Thompson, A. P., and Plimpton, S. J. (2008). A constant-time kinetic monte carlo algorithm for simulation of large biochemical reaction networks. *J. Chem. Phys.* 128, 205101

Stamatakis, M. (2014). Kinetic modelling of heterogeneous catalytic systems. *J. Phys. Condens. Matter* 27, 013001

Stamatakis, M. and Piccinin, S. (2016). Rationalizing the relation between adlayer structure and observed kinetics in catalysis. *ACS Catal.* 6, 2105–2111

Stamatakis, M. and Vlachos, D. G. (2011). A graph-theoretical kinetic monte carlo framework for on-lattice chemical kinetics. *J. Chem. Phys.* 134, 214115

Stamatakis, M. and Vlachos, D. G. (2012). Unraveling the complexity of catalytic reactions via kinetic monte carlo simulation: Current status and frontiers. *ACS Catal.* 2, 2648–2663

Stampfl, C., Kreuzer, H. J., Payne, S. H., Pfnür, H., and Scheffler, M. (1999). First-principles theory of surface thermodynamics and kinetics. *Phys. Rev. Lett.* 83, 2993–2996

Stegelmann, C., Andreasen, A., and Campbell, C. T. (2009). Degree of rate control: How much the energies of intermediates and transition states control rates. *J. Am. Chem. Soc.* 131, 8077–8082

Sutton, J. E., Guo, W., Katsoulakis, M. A., and Vlachos, D. G. (2016). Effects of correlated parameters and uncertainty in electronic-structure-based chemical kinetic modelling. *Nat. Chem.* 8, 331 – 337

Temel, B., Meskine, H., Reuter, K., Scheffler, M., and Metiu, H. (2007). Does phenomenological kinetics provide an adequate description of heterogeneous catalytic reactions? *J. Chem. Phys.* 126, 204711

Tolman, R. C. (1925). The principle of microscopic reversibility. *Proc. Natl. Acad. Sci. U. S. A.* 11, 436–439

van Kampen, N. G. (2007). *Stochastic Processes in Physics and Chemistry* (Amsterdam: North Holland), 3 edn.

Vignola, E., Steinmann, S. N., Vandegehuchte, B. D., Curulla, D., Stamatakis, M., and Sautet, P. (2017). A machine learning approach to graph-theoretical cluster expansions of the energy of adsorbate layers. *J. Chem. Phys.* 147, 054106

Vlachos, D. G. (2012). Multiscale modeling for emergent behavior, complexity, and combinatorial explosion. *AIChE J.* 58, 1314–1325

Voter, A. F. (2007). Introduction to the kinetic monte carlo method. In *Radiation Effects in Solids*, eds. K. E. Sickafus, E. A. Kotomin, and B. P. Uberuaga (Dordrecht: Springer Netherlands). 1–23

Voter, A. F., Montalenti, F., and Germann, T. C. (2002). Extending the time scale in atomistic simulation of materials. *Annu. Rev. Mater. Res.* 32, 321–346

Wang, S., Temel, B., Shen, J., Jones, G., Grabow, L., Studt, F., et al. (2011). Universal brønsted-evans-polanyi relations for c-c, c-o, c-n, n-o, n-n, and o-o dissociation reactions. *Catal. Lett.* 141, 370–373

1270 Wellendorff, J., Lundgaard, K. T., Møgelhøj, A., Petzold, V., Landis, D. D., Nørskov, J. K., et al. (2012).
1271   Density functionals for surface science: Exchange-correlation model development with bayesian error
1272   estimation. *Phys. Rev. B* 85, 235149

1273 Williams, I. H. and Maggiora, G. M. (1982). Use and abuse of the distinguished-coordinate method for
1274   transition-state structure searching. *J. Mol. Struct. THEOCHEM* 89, 365–378

1275 Wrigley, J. D. and Ehrlich, G. (1980). Surface diffusion by an atomic exchange mechanism. *Phys. Rev.*
1276   *Lett.* 44, 661–663

1277 Wu, C., Schmidt, D., Wolverton, C., and Schneider, W. (2012). Accurate coverage-dependence incorporated
1278   into first-principles kinetic models: Catalytic no oxidation on pt (111). *J. Catal.* 286, 88 – 94

1279 Xu, L. and Henkelman, G. (2008). Adaptive kinetic monte carlo for first-principles accelerated dynamics.
1280   *J. Chem. Phys.* 129, 114104

1281 Yang, L., Karim, A., and Muckerman, J. T. (2013). Density functional kinetic monte carlo simulation of
1282   water–gas shift reaction on cu/zno. *J. Phys. Chem. C* 117, 3414–3425

1283 Yu, B. D. and Scheffler, M. (1997). Physical origin of exchange diffusion on fcc(100) metal surfaces. *Phys.*
1284   *Rev. B* 56, R15569–R15572

1285 Zhang, Y., Blum, V., and Reuter, K. (2007). Accuracy of first-principles lateral interactions: Oxygen at
1286   pd(100). *Phys. Rev. B* 75, 235406

1287 Zimmerman, P. (2013). Reliable transition state searches integrated with the growing string method. *J.*
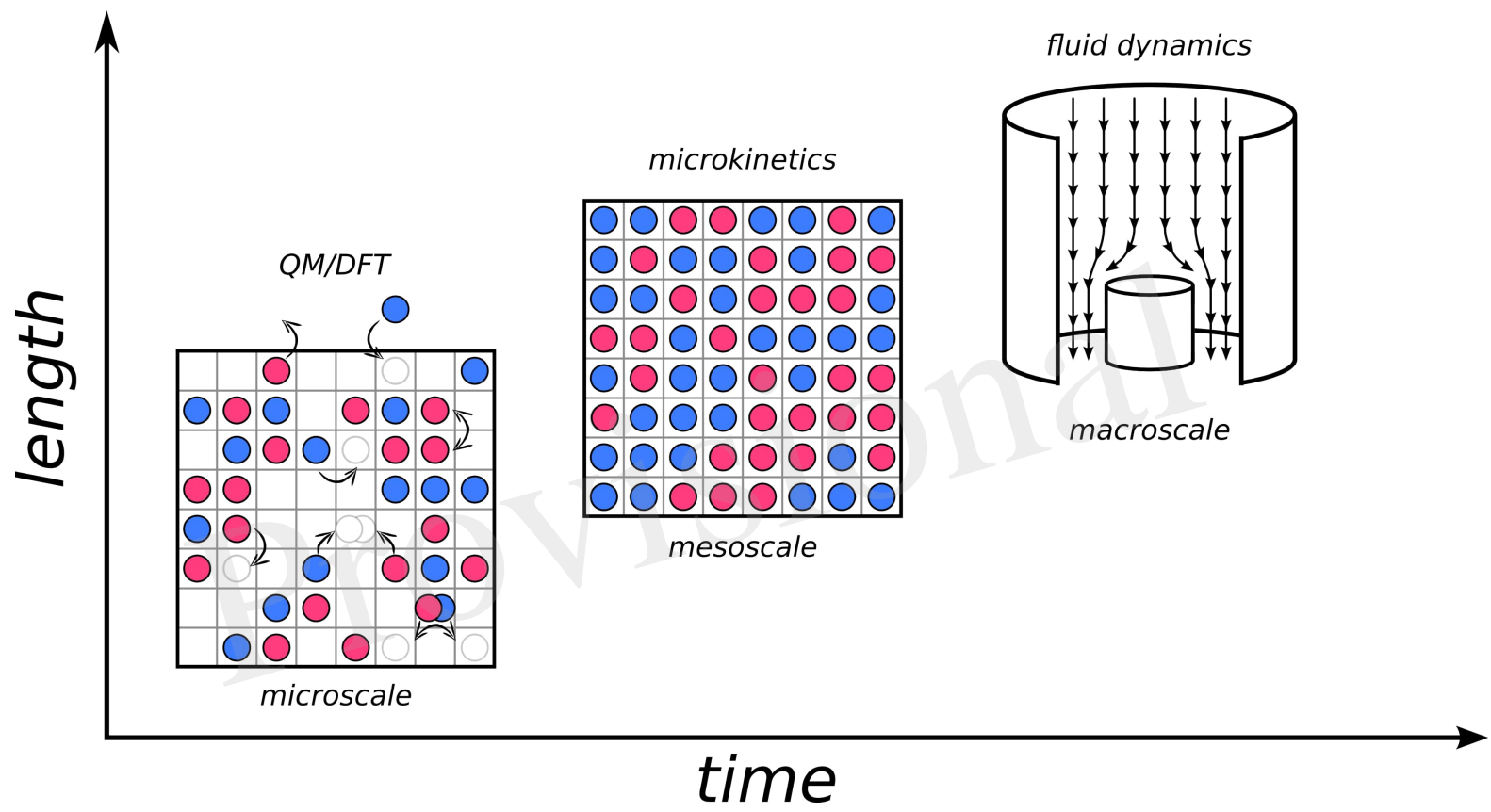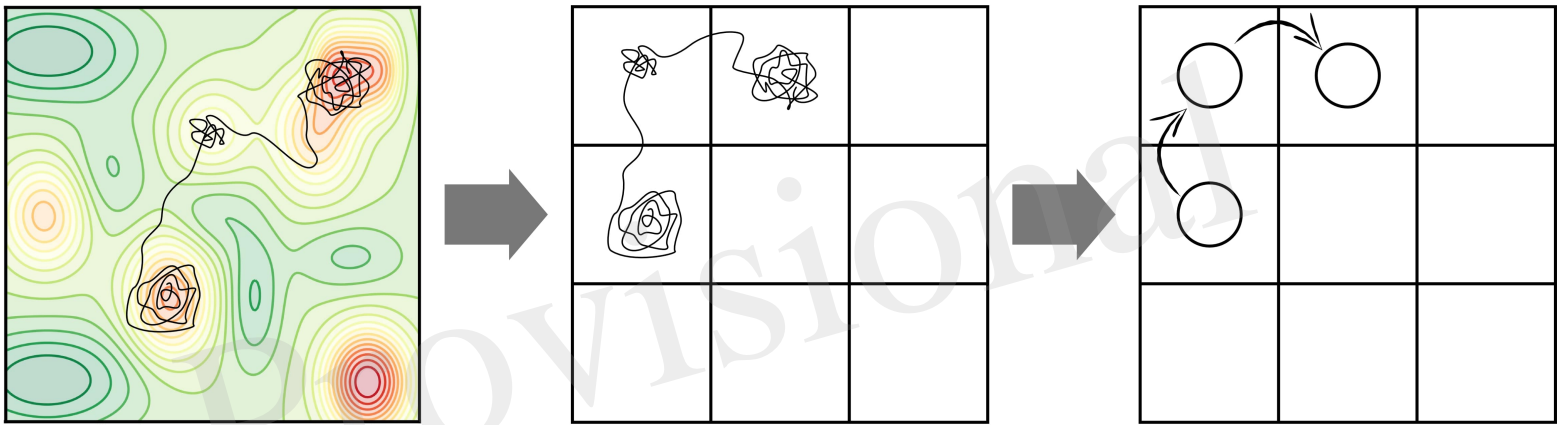1288   *Chem. Theory Comput.* 9, 3043–3050
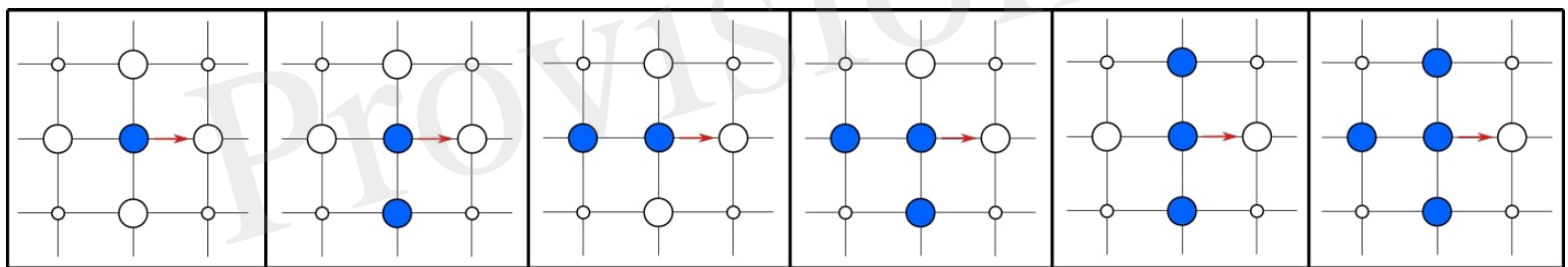
Figure 01.JPEG

Figure 02.JPEG

Figure 03.JPEG

Figure 04.JPEG

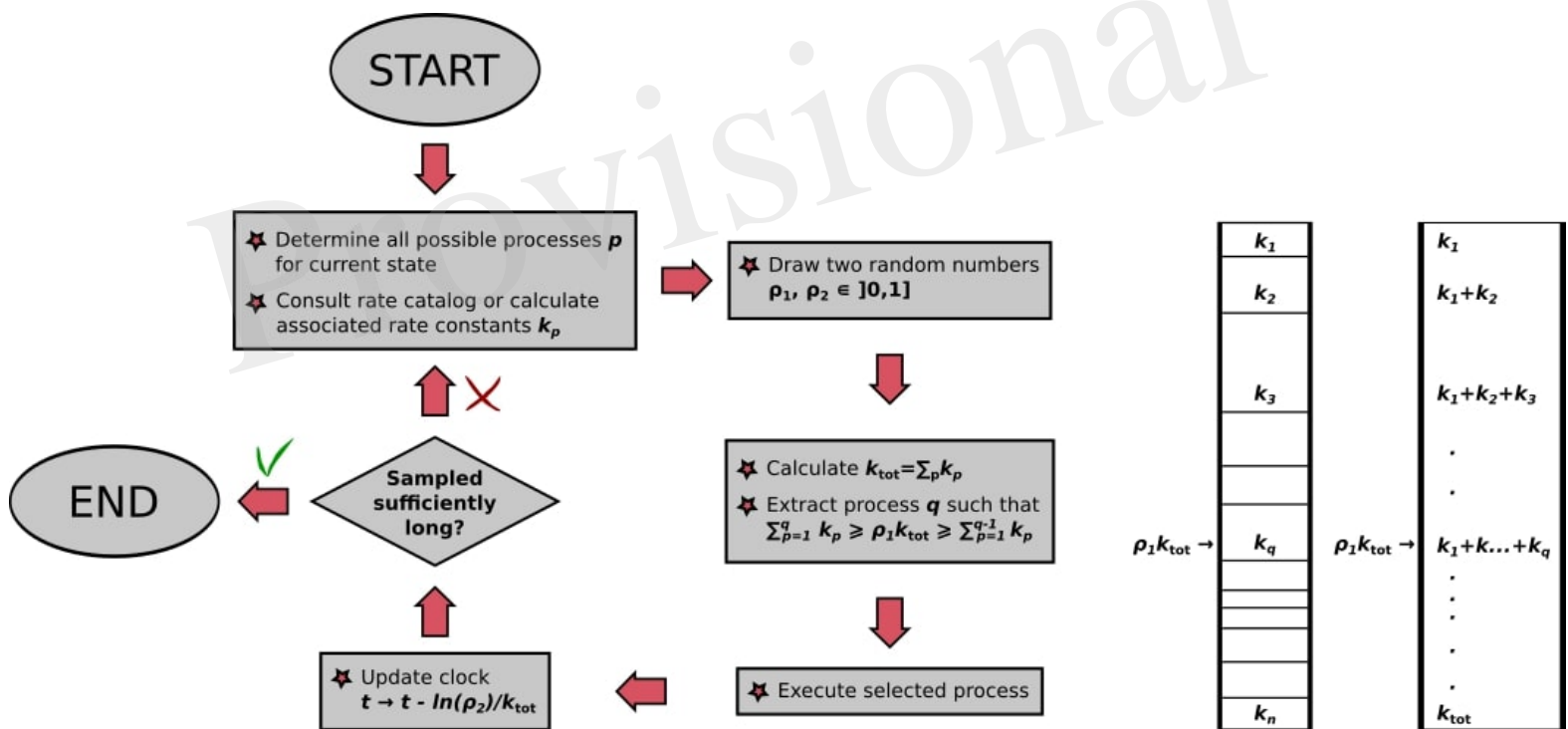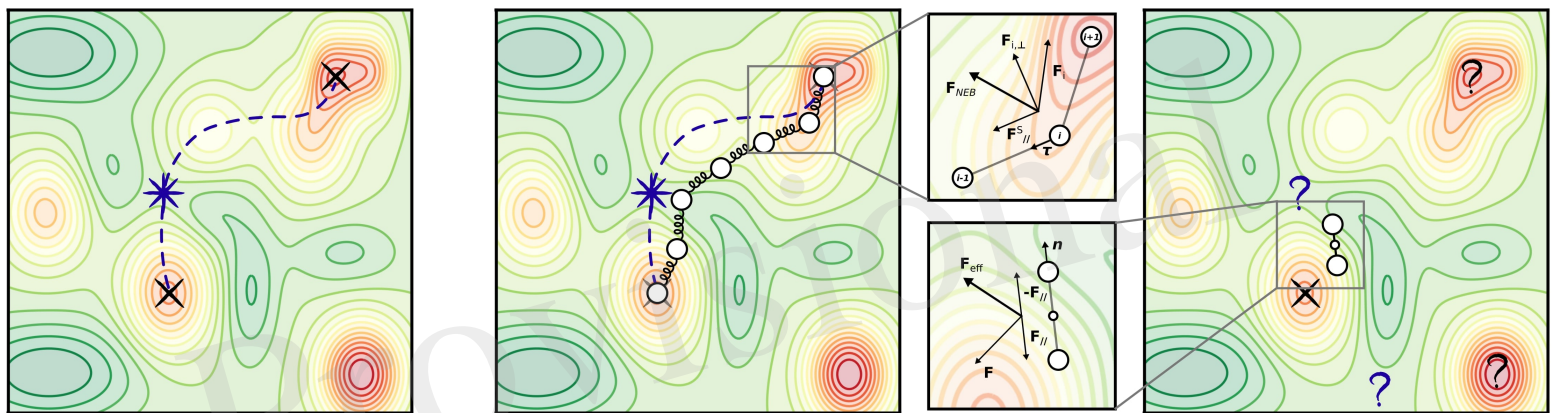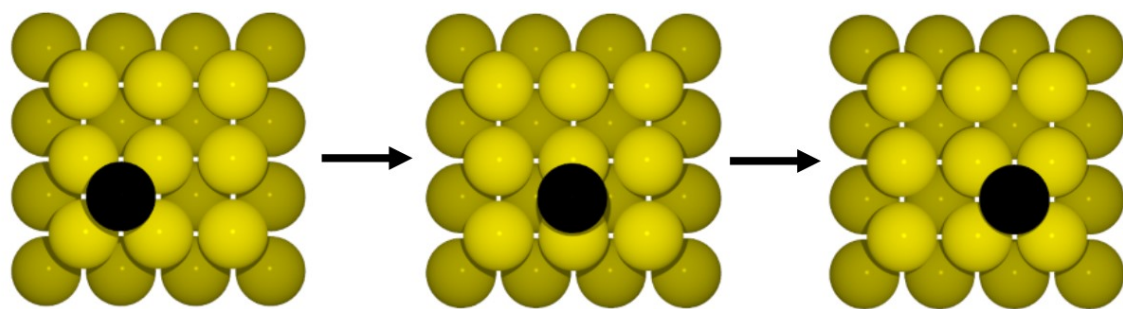Figure 05.JPEG

Figure 06.JPEG
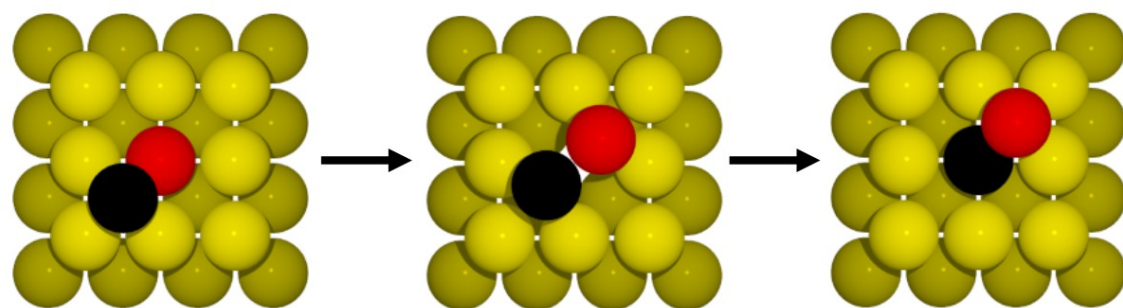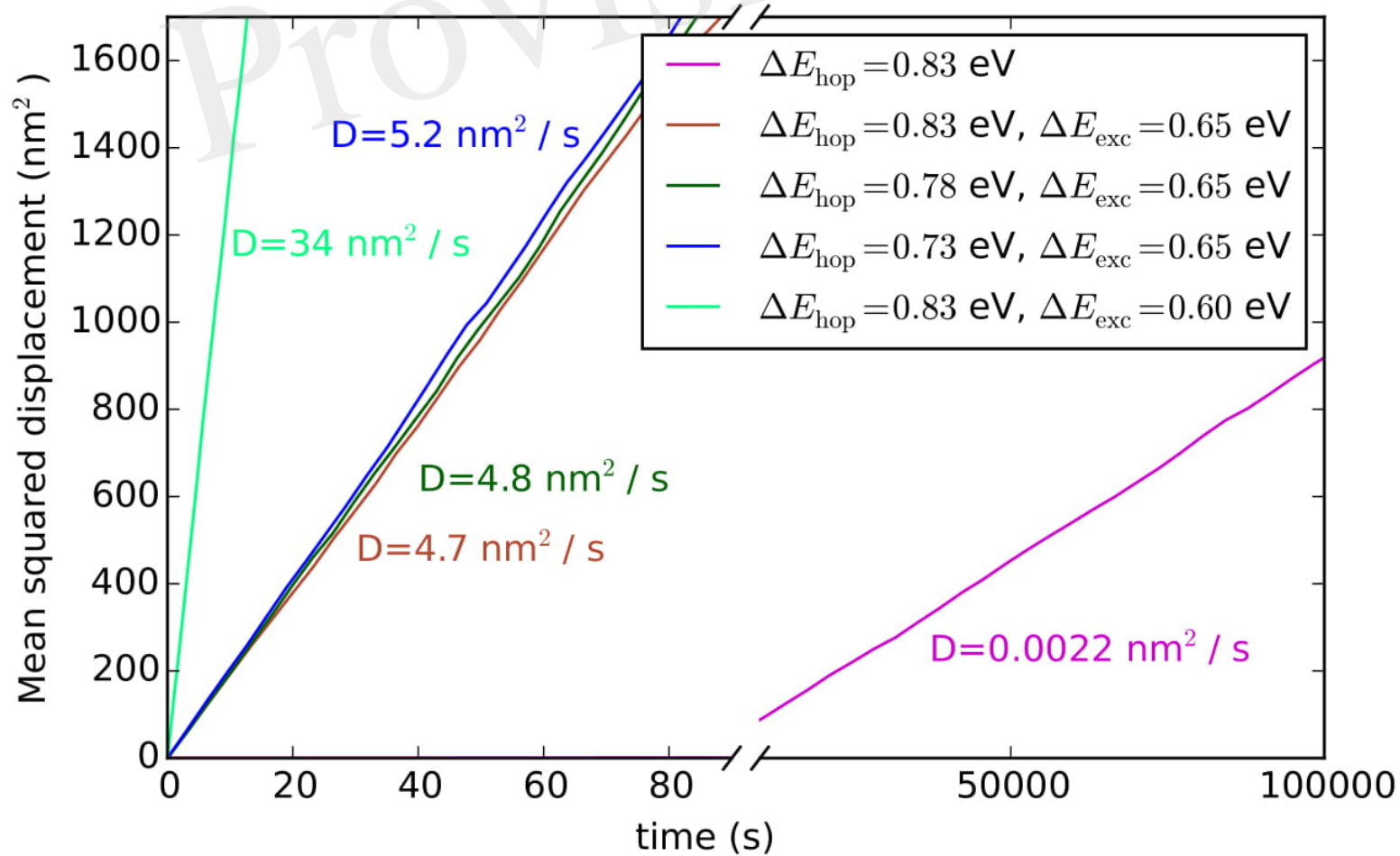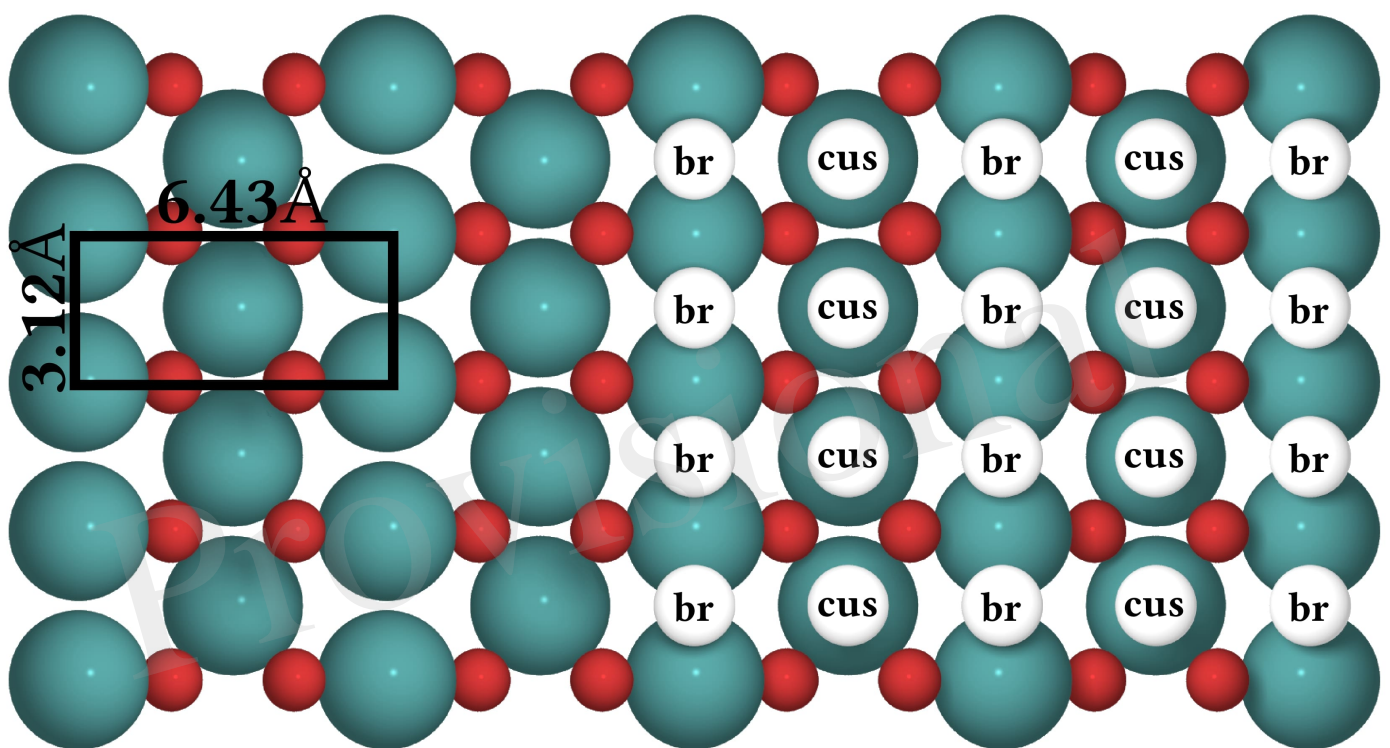
(a) Hopping diffusion

(b) Exchange diffusion
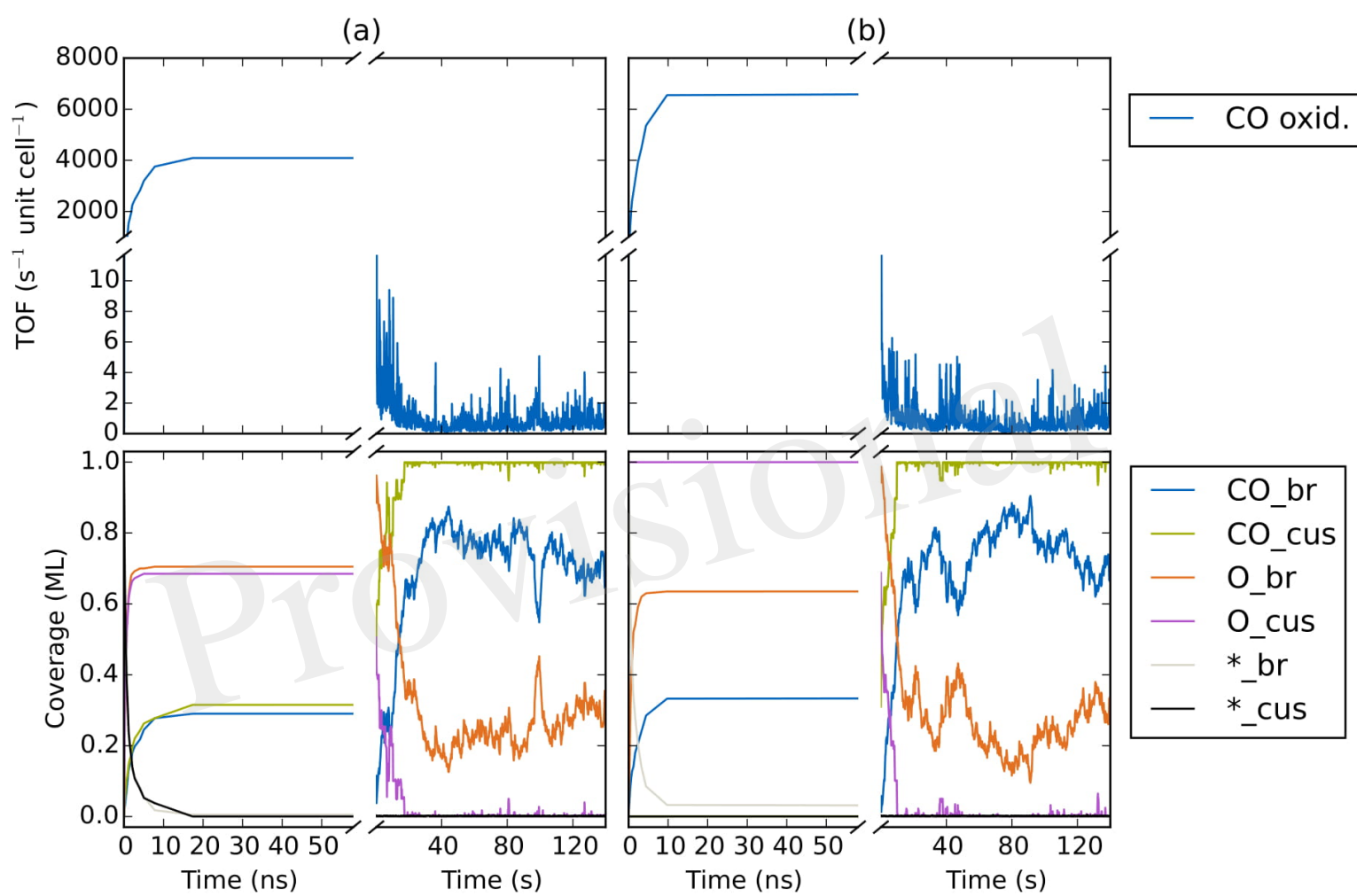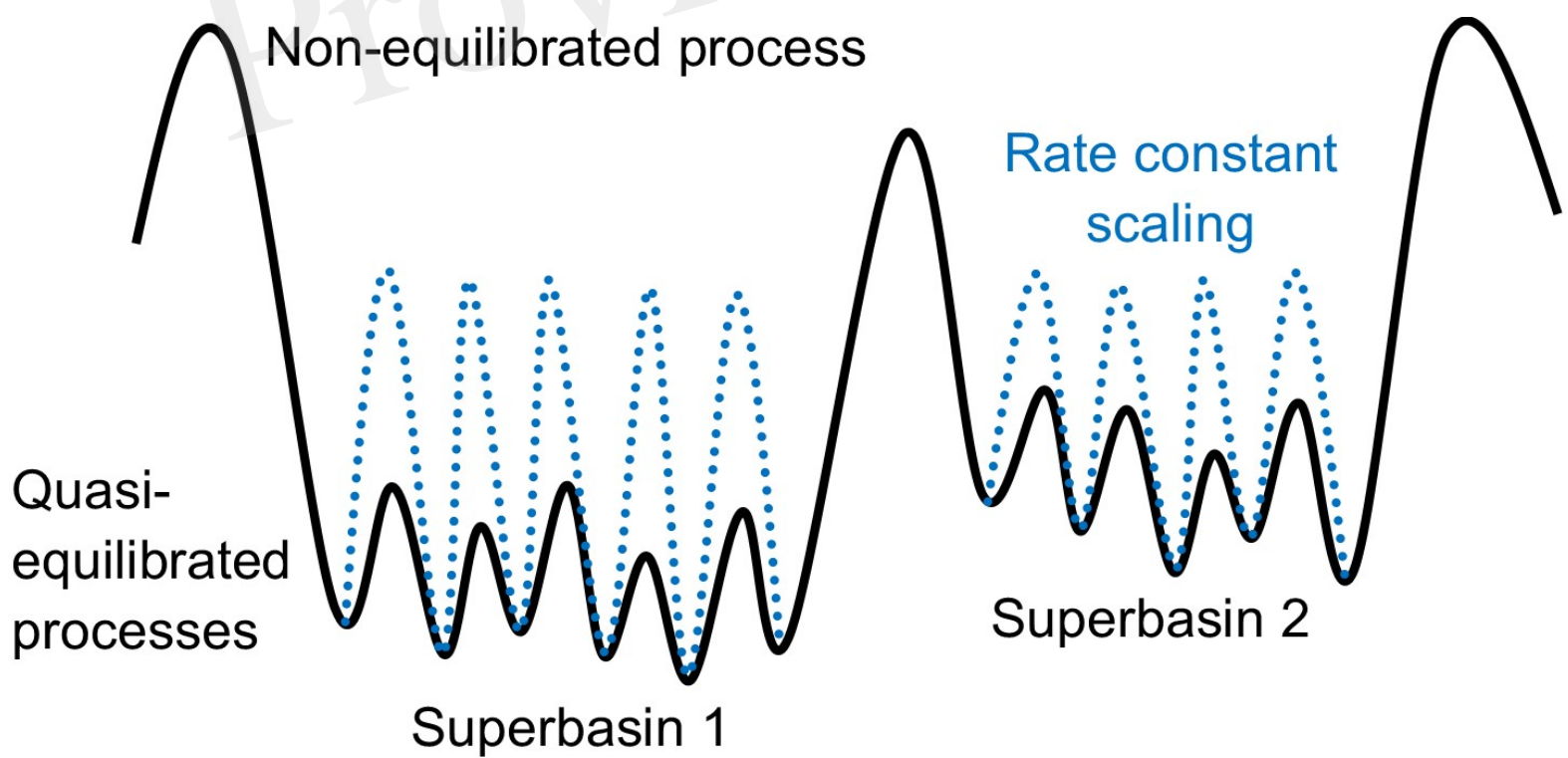
Figure 07.JPEG

Figure 08.JPEG

Figure 09.JPEG

Figure 10.JPEG

Non-equilibrated process

Rate constant scaling

Quasi-equilibrated processes

Superbasin 1

Superbasin 2

Figure 11.JPEG

(a) top view

y

x

empty

atom

empty
or
atom

side view

z

x

(b) T = 350 K   T = 450 K

(c) br cus br cus

br cus br cus

br cus br cus

(d) CO oxidation at RuO$_2$(110)

(50 x 50) lattice

rate catalog

on-the-fly

(10 x 10) lattice

Time per step [10^{-5} s]

Pairwise interactions